

11-14-2017

Genetic and Genomic Characterization of 462 Melanoma Patient-Derived Xenografts, Tumor Biopsies, and Cell Lines.

Bradley Garman
University of Pennsylvania

Ioannis N. Anastopoulos
University of Pennsylvania

Clemens Krepler
The Wistar Institute

Patricia Brafford
Follow this and additional works at: <https://jdc.jefferson.edu/willsfp>
The Wistar Institute

 Part of the [Oncology Commons](#), and the [Surgery Commons](#)

Katrin Sproesser
The Wistar Institute

[Let us know how access to this document benefits you](#)

Recommended Citation

See next page for additional authors

Garman, Bradley; Anastopoulos, Ioannis N.; Krepler, Clemens; Brafford, Patricia; Sproesser, Katrin; Jiang, Yuchao; Wubbenhorst, Bradley; Amaravadi, Ravi; Bennett, Joseph; Beqiri, Marilda; Elder, David; Flaherty, Keith T.; Frederick, Dennie T.; Gangadhar, Tara C.; Guarino, Michael; Hoon, David; Karakousis, Giorgos; Liu, Qin; Mitra, Nandita; Petrelli, Nicholas J.; Schuchter, Lynn; Shannan, Batool; Shields, Carol L.; Wargo, Jennifer; Wenz, Brandon; Wilson, Melissa A.; Xiao, Min; Xu, Wei; Xu, Xaiowei; Yin, Xiangfan; Zhang, Nancy R.; Davies, Michael A.; Herlyn, Meenhard; and Nathanson, Katherine L., "Genetic and Genomic Characterization of 462 Melanoma Patient-Derived Xenografts, Tumor Biopsies, and Cell Lines." (2017). *Wills Eye Hospital Papers*. Paper 78.
<https://jdc.jefferson.edu/willsfp/78>

This Article is brought to you for free and open access by the Jefferson Digital Commons. The Jefferson Digital Commons is a service of Thomas Jefferson University's [Center for Teaching and Learning \(CTL\)](#). The Commons is a showcase for Jefferson books and journals, peer-reviewed scholarly publications, unique historical collections from the University archives, and teaching tools. The Jefferson Digital Commons allows researchers and interested readers anywhere in the world to learn about and keep up to date with Jefferson scholarship. This article has been accepted for inclusion in Wills Eye Hospital Papers by an authorized administrator of the Jefferson Digital Commons. For more information, please contact: JeffersonDigitalCommons@jefferson.edu.

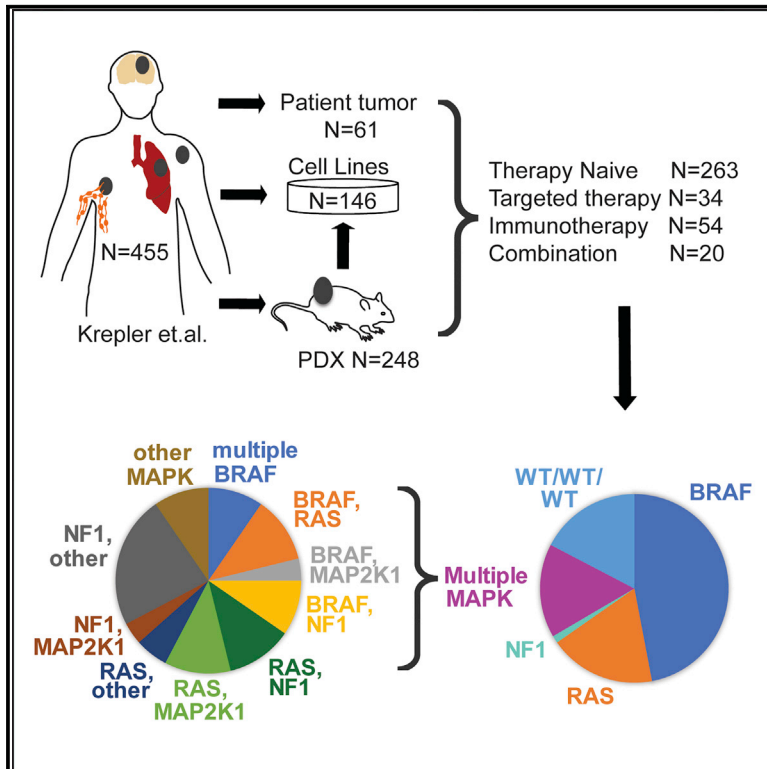
Authors

Bradley Garman, Ioannis N. Anastopoulos, Clemens Krepler, Patricia Brafford, Katrin Sproesser, Yuchao Jiang, Bradley Wubbenhorst, Ravi Amaravadi, Joseph Bennett, Marilda Beqiri, David Elder, Keith T. Flaherty, Dennie T. Frederick, Tara C. Gangadhar, Michael Guarino, David Hoon, Giorgos Karakousis, Qin Liu, Nandita Mitra, Nicholas J. Petrelli, Lynn Schuchter, Batool Shannan, Carol L. Shields, Jennifer Wargo, Brandon Wenz, Melissa A. Wilson, Min Xiao, Wei Xu, Xaiowei Xu, Xiangfan Yin, Nancy R. Zhang, Michael A. Davies, Meenhard Herlyn, and Katherine L. Nathanson

Cell Reports

Genetic and Genomic Characterization of 462 Melanoma Patient-Derived Xenografts, Tumor Biopsies, and Cell Lines

Graphical Abstract



Authors

Bradley Garman,
Ioannis N. Anastopoulos,
Clemens Krepler, ..., Michael A. Davies,
Meenhard Herlyn, Katherine L. Nathanson

Correspondence

knathans@upenn.edu

In Brief

Garman et al. have characterized melanoma PDXs and cell lines described in Krepler et al. (see the related paper in this issue of *Cell Reports*), identifying major and minor subtypes, some of which were previously not well defined, targeted and immunotherapy resistance, and tumor heterogeneity, creating a set of reagents for future drug discovery and biological studies.

Highlights

- Melanoma cell lines and PDXs more likely to be *BRAF/NRAS* mutant than patient tumors
- Mutations in melanoma PDXs are concordant with tumors from which they are derived
- Contrasting *MAPK* pathway mutation patterns: one high activity, several low activity
- Recurrent disease displays intra- and inter-tumor mutational heterogeneity



Genetic and Genomic Characterization of 462 Melanoma Patient-Derived Xenografts, Tumor Biopsies, and Cell Lines

Bradley Garman,^{1,16} Ioannis N. Anastopoulos,^{1,16} Clemens Krepler,² Patricia Brafford,² Katrin Sproesser,² Yuchao Jiang,³ Bradley Wubbenhorst,¹ Ravi Amaravadi,^{4,5} Joseph Bennett,⁶ Marilda Beqiri,² David Elder,^{5,8} Keith T. Flaherty,⁹ Dennie T. Frederick,⁹ Tara C. Gangadhar,^{4,5} Michael Guarino,⁶ David Hoon,¹⁰ Giorgos Karakousis,¹¹ Qin Liu,² Nandita Mitra,¹² Nicholas J. Petrelli,⁶ Lynn Schuchter,^{4,5} Batool Shannan,² Carol L. Shields,¹³ Jennifer Wargo,¹⁴ Brandon Wenz,¹ Melissa A. Wilson,¹⁵ Min Xiao,² Wei Xu,⁵ Xaiwei Xu,^{5,8} Xiangfan Yin,² Nancy R. Zhang,³ Michael A. Davies,⁷ Meenhard Herlyn,² and Katherine L. Nathanson^{1,5,17,*}

¹Department of Medicine, Division of Translational Medicine and Human Genetics, Perelman School of Medicine at the University of Pennsylvania, Philadelphia, PA, USA

²The Wistar Institute, Molecular and Cellular Oncogenesis Program, Tumor Microenvironment and Metastasis Program, and Melanoma Research Center, Philadelphia, PA, USA

³Department of Statistics, The Wharton School, University of Pennsylvania, Philadelphia, PA, USA

⁴Department of Medicine, Division of Hematology/Oncology, Perelman School of Medicine at the University of Pennsylvania, Philadelphia, PA, USA

⁵Abramson Cancer Center, Perelman School of Medicine at the University of Pennsylvania, Philadelphia, PA, USA

⁶Helen F. Graham Cancer Center at Christiana Care Health System, Newark, DE, USA

⁷Department of Melanoma Medical Oncology, University of Texas MD Anderson Cancer Center, Houston, TX, USA

⁸Department of Pathology and Laboratory Medicine, Perelman School of Medicine at the University of Pennsylvania, Philadelphia, PA, USA

⁹Department of Medicine, Division of Hematology & Oncology, Massachusetts General Hospital, Boston, MA, USA

¹⁰Department of Translational Molecular Medicine, John Wayne Cancer Institute, Providence Saint John's Health Center, Santa Monica, CA, USA

¹¹Department of Surgery, Perelman School of Medicine at the University of Pennsylvania, Philadelphia, PA, USA

¹²Department of Biostatistics, Epidemiology and Informatics, Perelman School of Medicine at the University of Pennsylvania, Philadelphia, PA, USA

¹³Ocular Oncology Service, Wills Eye Hospital, Thomas Jefferson University, Philadelphia, PA, USA

¹⁴Department of Surgical Oncology, University of Texas MD Anderson Cancer Center, Houston, TX, USA

¹⁵Perlmutter Cancer Center, NYU School of Medicine, NYU Langone Medical Center, New York, NY, USA

¹⁶These authors contributed equally

¹⁷Lead Contact

*Correspondence: knathans@upenn.edu

<https://doi.org/10.1016/j.celrep.2017.10.052>

SUMMARY

Tumor-sequencing studies have revealed the widespread genetic diversity of melanoma. Sequencing of 108 genes previously implicated in melanoma-genesis was performed on 462 patient-derived xenografts (PDXs), cell lines, and tumors to identify mutational and copy number aberrations. Samples came from 371 unique individuals: 263 were naive to treatment, and 108 were previously treated with targeted therapy (34), immunotherapy (54), or both (20). Models of all previously reported major melanoma subtypes (*BRAF*, *NRAS*, *NF1*, *KIT*, and *WT/WT/WT*) were identified. Multiple minor melanoma subtypes were also recapitulated, including melanomas with multiple activating mutations in the MAPK-signaling pathway and chromatin-remodeling gene mutations. These well-characterized melanoma PDXs and cell lines can be used not only as reagents for a large array of biological studies

but also as pre-clinical models to facilitate drug development.

INTRODUCTION

Although cancer incidence overall declined in the United States from 2002 to 2011, the incidence rates of melanoma continue to rise (Ryerson et al., 2016). If diagnosed early, surgical resection is curative in most melanoma patients. However, roughly 20% of patients will develop metastatic disease. Melanoma accounts for approximately 50,000 deaths per year worldwide, over 75% of skin cancer-related mortality (Corrie et al., 2014). With the cost of massively parallel sequencing technologies decreasing at a rapid rate, precision medicine is routinely practiced, in which the genetic profile of a patient's melanoma is obtained and used to guide diagnosis and treatment. This practice is particularly valuable for melanoma due to the malignancy's severity and the availability of effective targeted therapies for common mutations (Robert et al., 2015).

Melanoma is characterized by constitutive activation of the mitogen-activated protein kinase (MAPK)- and/or

phosphoinositide 3-kinase (PI3K)-signaling pathways and disruption of the cell cycle. Approximately 45% of melanomas harbor an activating mutation affecting codon 600 of the serine/threonine-protein kinase BRAF (*BRAF* V600E), against which targeted inhibitors (BRAFi) were developed (Davies et al., 2002; Chapman et al., 2011; Krepler et al., 2016). BRAFis provide clinical benefit to a large percentage of advanced melanoma patients whose tumors harbor a *BRAF* V600E mutation. However, median progression-free survival is approximately 6 months (Chapman et al., 2011; Hauschild et al., 2012). Combining BRAFi with MEK inhibitor (MEKi) therapy increases responses rates and approximately doubles median progression-free survival (Robert et al., 2015). Nevertheless, drug resistance is still a major hurdle in the long-term management of melanoma with targeted therapies (Wagle et al., 2014). Simultaneously, immune checkpoint inhibitors have been increasingly used for melanoma treatment. These agents (anti-CTLA-4, anti-PD-1, and anti-CTLA-4/anti-PD1) have demonstrated increasing rates of responses in clinical trials, many of which are durable (i.e., >2 years) (Larkin et al., 2015). Targeted and immunotherapy combinations are currently being explored.

In recent years, several large-scale massively parallel sequencing studies have provided valuable insights into the genetics of melanoma. Initial whole-exome sequencing studies demonstrated that *NF1*, *ARID2*, *PPP6C*, *RAC1*, *SNX31*, *TACC1*, and *STK19* are significantly mutated genes in melanoma (Hodis et al., 2012; Krauthammer et al., 2012). The Cancer Genome Atlas Skin Cutaneous Melanoma (SKCM-TCGA) exome sequencing dataset identified several additional significantly mutated melanoma genes, namely, *MAP2K1*, *IDH1*, *RB1*, and *DDX3X* (Cancer Genome Atlas Network, 2015). The same groups classified melanomas into genetic subtypes as follows: *BRAF* mutant, *RAS* mutant, *NF1* mutant, and the triple wild-type (WT/WT/WT). Rare, low-frequency, driver mutations were identified in the WT/WT/WT subtype in *KIT*, *CTNNB1*, *GNA11*, and *GNAQ*. Additionally, an apparent increase in copy number variation (CNV) frequency in WT/WT/WT, particularly copy number amplifications, was detected in driver genes. Further, whole-exome sequencing studies revealed that *NF1* mutant melanomas frequently carry additional mutations in other MAPK-signaling pathway genes (Krauthammer et al., 2015; Arafah et al., 2015).

As sequencing of patient tumors continues to reveal the widespread genetic variability of melanomas, there is a critical need for genetically annotated melanoma translational models that accurately recapitulate the biology and molecular characteristics of the patient's original tumor for use in pre-clinical studies to develop personalized treatment strategies. We sequenced genes previously implicated in melanomagenesis to evaluate mutations and copy number changes in 115 human melanoma cell lines, 248 patient-derived xenografts (PDXs), 31 cell lines derived from PDXs (PDX CLs), and 68 patient tumors (462 samples total). Of the patients with melanoma, 263 were treatment naive and 54 were previously exposed to immunotherapy with anti-CTLA-4 or anti-PD-1, 34 to targeted therapy with BRAFi and/or MEKi, and 20 to a combination of targeted and immunotherapy.

RESULTS

Demographic and Clinicopathological Characteristics of Sequenced Cell Lines, PDXs, Patient Tumors, and PDX CLs

Sequencing was performed on cell lines, PDXs, and patient tumors. Of 115 Wistar Melanoma cell lines generated at the Wistar Institute, partial characterization has been reported on a subset (Hoek et al., 2006; Lin et al., 2008), and 31 additional lines were developed from PDX models. A further 314 tumor samples representing 253 individuals were either made into PDXs or directly sequenced from patients treated at the University of Pennsylvania (UPENN, 112), MD Anderson Cancer Center (MDACC, 86), Massachusetts General Hospital (23), Helen F. Graham Cancer Center (17), Jefferson (2), John Wayne Cancer Institute (8), Wills Eye Institute (4), and University of Duisburg-Essen (1). Three patients (1%) had stage II melanoma, 34 (7%) patients had stage III, 106 (42%) patients had stage IV, and for 115 (45%) the patient's stage at biopsy was unknown. Clinicopathological characteristics are summarized in Table S1; further details can be found in the companion paper (Krepler et al., 2017). Twenty-two samples (6% of unique cohort) were non-cutaneous melanomas, with mucosal (10, 3%), acral cutaneous (7, 2%), and uveal (5, 1%) primaries included.

Variability among Cell Lines, PDXs, PDX CLs, and Patient Tumors

Tumors were sequenced on a custom capture panel of 108 genes (MEL V1) known to be important in melanomagenesis (Table S2). The full genes (exons and introns) were sequenced for tumor suppressors to facilitate copy number calling, with a few exceptions. Exons only were sequenced for oncogenes. We developed an in-house annotation pipeline to classify variants as deleterious, likely deleterious, and of unknown significance (see the Experimental Procedures and Figure S1). Variants and copy number alterations (CNAs) were identified in all 108 targeted genes. A subset (101) was sequenced on a 119-gene panel (MEL V2) (Table S3); 106 genes were shared with MEL V2. Of 101 samples (36 unique patients), 45 were sequenced on both panels, enriched for non-*BRAF* V600E/K/D and non-*NRAS* Q61 mutant samples. The deleterious/likely deleterious variant concordance rates of MEL V1 and MEL V2 were 94% (217 of 231 MEL V1 variants found on MEL V2) and 97% (217 of 223 MEL V2 variants found on MEL V1) (Figure S2). Testing results for mutations in the major driver melanoma genes (*BRAF*, *RAS*, *NF1*, and *KIT*) did not differ.

Following variant calling, all 115 cell lines harbored at least one deleterious mutation, compared to 236 of 248 PDXs (95%), 30 of 31 PDX CL (97%) samples, and 59 of 68 patient tumors (87%). Likely deleterious mutations were found in 69 of 115 cell lines (60%), 168 of 248 PDXs (67%), 18 of 31 PDX CLs (58%), and 36 of 68 patient tumors (53%). Variants of unknown significance (VUSs) were found in 103 of 114 cell lines (90%), 222 of 248 PDXs (93%), 27 of 31 PDX CLs (87%), and 55 of 68 patient tumors (81%). Table S5 lists all called variants in our cohort. Among all four sample types, the total number of calls (deleterious/likely deleterious/VUS) did not differ significantly (Figure 1B). However, the alternate allele fractions (AAFs) of variants detected across

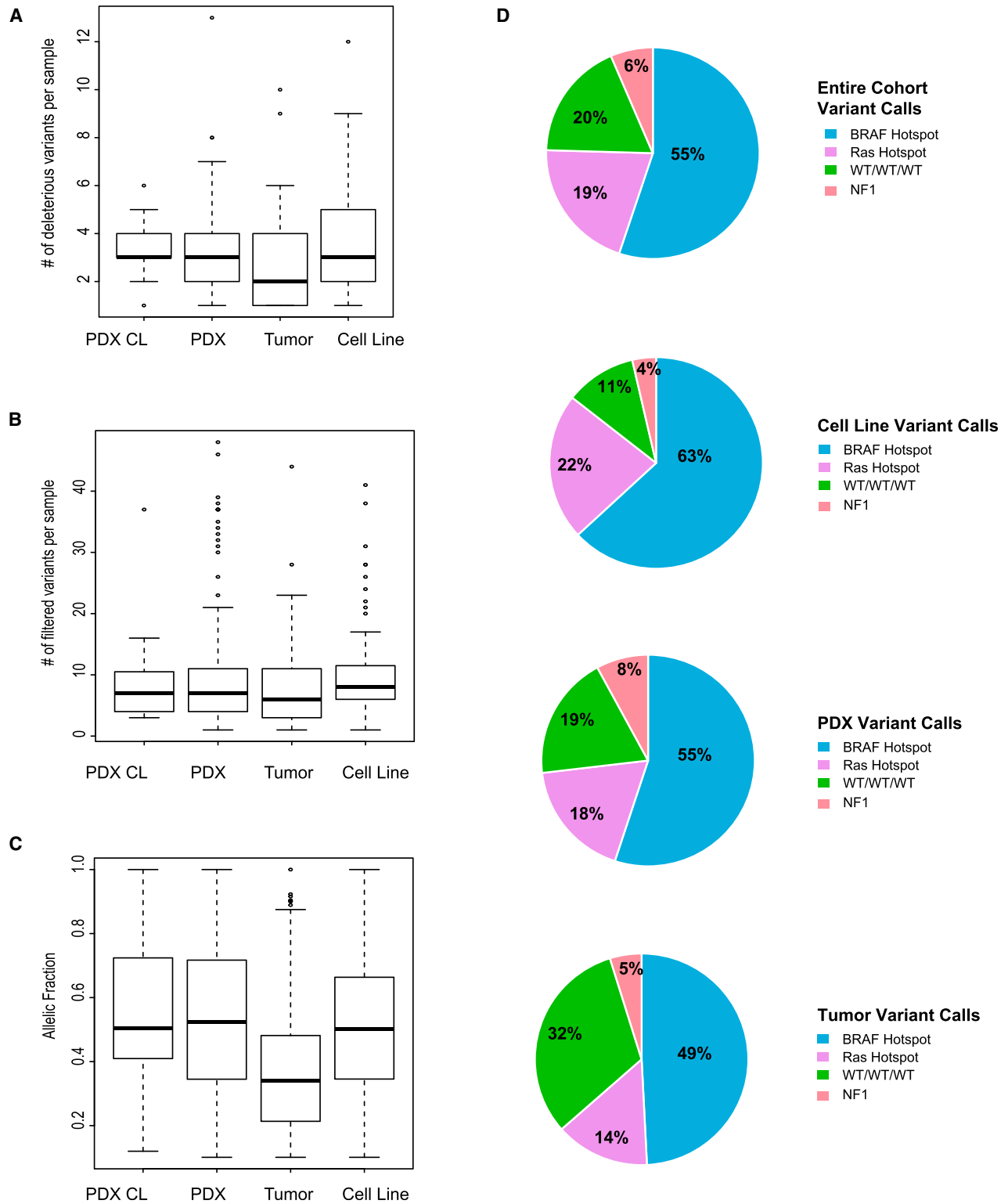


Figure 1. Variability among Four Different Sample Types (PDX CL, PDX, Patient Tumor, and Cell Line)

(A) Average number of deleterious variants detected per sample.

(B) Average number of total filtered variants detected per sample.

(C) Allelic fractions across the four sample types.

(D) Major subtypes (*BRAF* hotspot, *RAS* hotspot, *NF1* hotspot, and WT/WT/WT) and their differential distribution among the entire cohort.

all sample types were statistically significant different ($p = 2.2 \times 10^{-16}$). Patient tumors had the lowest AAF, presumably due to admixture with non-tumor cells, and PDX CLs had the highest AAF (Figure 1C).

We compared the prevalence of common mutations across the four sample types. In the samples from the 371 unique individuals, 203 (55%) had mutations in *BRAF*, 72 (19%) in *RAS* (*NRAS* and *KRAS*), and 22 (6%) in *NF1* (Figure 1D). As discussed in detail below, some samples had mutations in more than one of these genes, and for this purpose they were included in the most prevalent mutation group (e.g., those with *BRAF* and *RAS* mutations in the *BRAF* mutant group and those with *RAS* and *NF1* mutations in the *RAS* group). Seventy-four samples (20%) did not have mutations in the above genes (WT/WT/WT); 14 WT/WT/WT were non-cutaneous melanomas (acral [1, 1%], mucosal [9, 12%], or uveal [4, 6%]). For nine WT/WT/WT tumor biopsies, the sample provided may have been normal tissue, as we only identified one to three VUSs at 50% allele frequency in each; four did not grow in mice and five have not been tested for growth. Cell lines had a higher prevalence of both deleterious *BRAF* and *RAS* mutations than PDXs and patient tumors ($p = 0.05$; Figure 1D). *CDKN2A* mutations and homozygous deletions occurred at a higher frequency (74, 68%) in cell lines, compared to 104 (52%) PDXs and 14 (24%) tumors ($p = 3.3 \times 10^{-7}$). *TP53* mutations and homozygous deletions also occurred at a higher frequency in cell lines (34%), as compared to PDXs (23%) and tumors (21%), but not significantly. The distribution of mutations in PDXs and tumors was reflective of what has been reported previously (Cancer Genome Atlas Network, 2015). In contrast, cell lines were significantly more likely to be *BRAF* or *RAS* mutant with loss of *CDKN2A*, likely reflecting difficulties establishing cell lines from *NF1* mutant or WT tumors.

Prevalence of Gene Mutations and Predicted Copy Number Changes

Among all sequenced samples (462), we identified deleterious/likely deleterious mutations in 101 of 108 genes. To summarize the prevalence of gene mutations, the percentage of unique patients (371) was calculated. Deleterious mutations were most prevalent in our cohort in the following genes: *TERT* promoter region (215, 62.5% of all samples), *BRAF* (200, 58.1%), *NRAS* (81, 23.51%), *TP53* (63, 18.3%), *CDKN2A* (49, 14.2%), *NF1* (35, 10.2%), *ARID2* (28, 8.1%), and *PTEN* (20, 5.8%) (Figure S3A). Likely deleterious mutations were most frequently detected in the following: *DCC* (32, 19% of all samples), *GRM3* (30, 17.9%), *PTPRP* (19, 11.3%), *PREX2* (19, 11.3%), *GRIN2A* (19, 10%), and *PTEN* (17, 10.1%) (Figure S3B). Variants were not detected in *CD274*, *MDM4*, *SDHD*, or *SMARCB1*.

Of the 371 unique samples, 294 unique samples (79%) had a homozygous loss or high amplification in at least one gene. The mean (and range) of the number of highly amplified (copy number > 3.3) and homozygously deleted genes per sample was 1 (0 to 5) and 2 (0 to 8), respectively. The most frequently highly amplified genes were the following: *CDK6* (91, 30%), *MET* (79, 26.1%), *DDX3X* (69, 22.8%), *BRAF* (68, 22.4%), *DYNC111* (55, 18.2%), *EZH2* (51, 16.8%), *MITF* (49, 16.2%), *MYC* (45, 14.9%), *PREX2* (45, 14.9%), *STK19* (43, 14.2%), and *NOTCH2* (30, 10%) (Figure S3C). The genes most frequently

homozygously deleted were the following: *CDKN2A* (130, 65.3%), *CDKN2B* (102, 51.3%), *PTEN* (47, 23.6%), and *TP53* (12, 6%) (Figure S3D). A complete list of CNAs can be found in Table S6.

MAPK-Signaling Pathway Mutations

The mutational landscape of our samples revealed two distinct patterns of mutations within the MAPK-signaling pathway: (1) single-hotspot *BRAF* or *NRAS* mutations; and (2) multiple non-hotspot variants across different genes encoding proteins within the MAPK-signaling pathway, including *NF1* mutations. Across our naive and immunotherapy cohort (317 patients, 85% of unique cohort), 206 melanomas representing unique individuals (65% of naive and immunotherapy cohort) followed pattern 1; 148 had solitary driver mutations in *BRAF* (72%) and 58 (28%) in *NRAS*. Pattern 2 melanomas representing 52 unique individuals (14% of unique; 16% of naive and immunotherapy cohort) had more than one deleterious or likely deleterious mutation in either a MAPK-signaling gene or in a gene encoding an effector protein of the MAPK pathway, as shown in Table 1. Three pattern 2 samples were acral (2) and mucosal (1). Eighteen samples harbored a deleterious or likely deleterious non-V600 *BRAF* mutation (p.H57Y, p.G464E, p.S465Y, p.G466E, p.G469E, p.L496V, p.N581S, p.N581Y, p.D594G, p.V624F, p.K601E, and p.600_601del) (Figure S4). We also noted an additional six non-V600 *BRAF* mutations, which we designated as VUSs but that may have functional significance (p.G7S, p.F294L, p.S365L, p.S365L, p.A497V, and p.T740A). We also identified five *BRAF* non-V600 variants (p.G9A, p.L505H, p.P318S, p.P328S, and p.A366P) in samples also carrying V600E mutations, which are less likely to be functional. All non-V600 *BRAF* mutations had concurrent deleterious/likely deleterious mutations or high-level amplifications in other MAPK-signaling genes. Co-occurring *RAS* deleterious mutations were most frequent, found in 60% of non-hotspot *BRAF* mutant samples as compared to 2%, 6.3%, and 21.5% of those with *BRAF* V600E, V600K, and other *BRAF* hotspot mutations, respectively ($p < 0.0001$). Most melanomas had a single second deleterious mutation in a MAPK-signaling gene; a few had three. We identified concurrent mutations or amplifications in other MAPK-signaling pathway genes in all *BRAF* non-V600 codon mutations, except for one, which had incomplete sequencing.

Twenty-three *RAS* mutants had co-occurring mutations in the MAPK-signaling pathway (Table 1; Figure S4), and, therefore, they fell into pattern 2, compared to 58 pattern 1 *RAS* mutant samples (53, 91% Q61; 5, 9% non-Q61). Eleven Q61 (17% of all Q61) and 13 non-Q61 (75% of all non-Q61) mutated melanoma samples harbored additional mutations in the MAPK-signaling pathway ($p = 2.2 \times 10^{-16}$ for enrichment of non-Q61 mutations). Of the 30 *NF1*-mutated melanomas, 26 (87%) harbored concurrent deleterious/likely deleterious MAPK-signaling pathway mutations (Table 1). Two of the remaining four *NF1*-mutated melanomas had VUSs in *MAP3K5* (WM4242 also had a deleterious mutation in *ROS1* [c.780-1G > A]). Of the four possible mutations observed in *RASA2* (one truncating and three likely deleterious missense), only two were observed in *NF1* mutant samples. Four of nine (44%) *KIT* mutant samples also carried concurrent MAPK pathway mutations.

Table 1. Samples with Co-occurring Mutations in the MAPK-Signaling Pathway

Sample	Sample Type	Hotspot BRAF	Non-V600 BRAF	RAS	NF1	KIT	MAP2K1	MAP2K2	MAP3K5	MAP3K9	STK19	RASA2	SOS1	SOS2	RAF1	PTPN11	SPRED1
WM3929	PDX CL	V600E	K52Y														
RL159	Cell Line		K601E				E203K										
WM4478	Patient biopsy		K601E														
WM4365	PDX		486_491del				P124R										
C8161	Cell Line		G464E	KRAS	G12D												
WM3670	Cell Line		G469E	KRAS	G12D												
WM4088	PDX		G469E	KRAS	G12D												
WM3929	Cell Line		D599G	KRAS	G12D												
WM4231-2	PDX		V624F	KRAS	Q61R												
WM4077	PDX		S465Y	KRAS	G13D	W561X											
WM1963	Cell Line		N581S	KRAS	A146T	Q531X		D67N									
WM4455	Patient biopsy		L495V			Q353X											K360X
WM4516	Patient biopsy		G466E			Q543X; L2315F			Q1211X								
WM3912	Cell Line		N391Y			37fs; T165fs				R160C							
WM4342	PDX		H574Y			Q2616X; K2456X			G1006X			S590L					Q245X
WM4223	PDX		D594G														
WM4508	Patient biopsy		600_601del														
WM3792	Cell Line		600_601del														
WM4257	PDX			KRAS	Q61K	Q1763X; 889-2A>C											P312S
WM4369	PDX			KRAS	G13D	L626fs											
WM4550	Patient biopsy			KRAS	G13V	S1599F											
WM4233	PDX			KRAS	Q61H	R440X											
WM3681	Cell Line			KRAS	G13N	Q519X; T185+1G>A											
RC6041	PDX			KRAS	G13V	Q1622X; G1166fs				960+1G>T							
WM4272	PDX			KRAS	Q61K					P124S							
WM3974	PDX			KRAS	G12A		L576P			C121S							
WM4430	PDX			KRAS	Q61R					E144K							
WM4542	Patient biopsy			KRAS	Q61R					P124S							
WM4549	PDX			KRAS	Q61R					S231L							
WM4327	PDX			KRAS	Q61R					E144K							
WM4273	PDX			KRAS	Q61L												
WM4451	PDX			KRAS	G12D					Q1289X							E385X
WM4528	Patient biopsy			KRAS	Q61K							W258R					
M450	Cell Line					K395fs; N734fs				R174C		Q616X				p.33Y	
WM4073	PDX					F1357fs						R75C					
WM4314	PDX					Q236X			A52V								
WM4274	PDX					K1459N			P124S								
WM4082	PDX					L1892fs											
MEWO	Cell Line					Q1338X				1588-1G>A							
WM4281	PDX					R1362X; Q684X				R560X							
D24	Cell Line					R1958C				R160C							
WM4499	Patient biopsy					Q392X				E319K							
WM4359-1	PDX					Q1756X									M267R		
WM4443	PDX					Q1174X; W223X									R676C		
WM4287	PDX					Q238X; 5609+1G>A											E478K
WM4260	PDX					1166_1170del	K642E										
WM4210-2	PDX					R440X	K642T										
WM4565	Patient biopsy						K642E										I320fs
WM4286	PDX								E203K								
WM4447	Patient biopsy								F330L								
TH202	PDX							P269L									
WM4254	PDX									E477X							

Green, high-level amplification (>3.3 fold); red, deleterious mutations; blue, likely deleterious mutations; gray, samples and genes not sequenced on the 119-gene panel; purple, loss of wild-type allele; peach, non-cutaneous melanoma.

Four wild-type (WT/WT/WT) samples in this cohort harbored likely deleterious and deleterious mutations in *MAP2K1/2* and *MAP3K5*, including one with a truncating deleterious mutation in *MAP3K5* (p.E477X) (Figure S5).

Genetic/Genomic Landscape of Sequenced Naive Melanoma Cell Lines, PDXs, PDX CLs, and Patient Tumors

Deleterious mutations, homozygous losses, and high-level copy number amplifications in the 225 naive-to-treatment samples are shown in Figure 2; only one sample from each patient is included. Likely deleterious mutations and other genomic aberrations also are included in Figure S6. As deleterious *TERT* promoter mutations (Table S4) were detected in 67% of samples, and ubiquitously in all subtypes, they are not included in Figures 2 and S6A.

Within *BRAF*-V600E mutant treatment-naive samples, we observed previously well-described subtypes. Of 105, 44 (42%) *BRAF* V600E-mutated samples from unique patients harbored truncating and/or deleterious missense mutations in cell cycle genes (*CDKN2A*, *CDK4*, and/or *TP53*). The remaining 61 (58%) *BRAF* V600E-mutated samples had more frequent homozygous loss of *CDKN2A/B* (46% versus 25%; $p = 0.03$), but not *PTEN* (25% versus 11%). Homozygous deletions in *PTEN* occurred almost exclusively in *BRAF* V600E samples (91%) ($p < 0.0001$). Within the subset of *BRAF* V600E-mutated

samples lacking additional *CDKN2A*, *CDK4*, and/or *TP53* mutations, 10 samples (9.5% of unique patients) lacked the C > T nucleotide substitution pattern characteristic of UV sun damage (Brash, 2015), possibly due to low mutation burden. *NF1* mutant samples had the highest overall mutational burden of all subtypes ($p = 1 \times 10^{-6}$), the majority of which were C > T transitions. Of 11 *NF1* mutant samples from unique patients, seven samples (64%) harbored a deleterious mutation in *TP53*, more frequently than in other subtypes ($p = 0.003$). Ten of 29 WT/WT/WT (34.5%) harbored previously reported rare mutations in *GNAQ*, *GNA11*, and *CTNNB1*, in a mutually exclusive fashion, six of which were uveal PDX and cell lines. A further two WT/WT/WT samples (7%) were acral and mucosal melanomas.

Multiple samples displayed high-level copy number amplifications. Of 27, 19 (70%) high amplifications in *MITF* occurred in *BRAF* V600E-mutated samples. Of the 12 co-occurrences of high amplification in *FGF3/4* and/or *CCND1*, nine (75%) also harbored high amplification in *MITF*. *FGF3*, *FGF4*, and *CCND1* are co-localized at 11q13.3, explaining co-occurrence, whereas *MITF* is on chromosome 3, suggesting a synergistic effect. Of 31, 25 (80.6%) concurrent amplifications in *BRAF*, *MET*, and/or *EZH2* occurred in *BRAF* hotspot mutant samples ($p = 0.009$). Three very high-level *BRAF* amplification events (6- to 16-fold) were identified, two of which were in *BRAF* V600K mutants. Finally, 14 of 24 (58%)

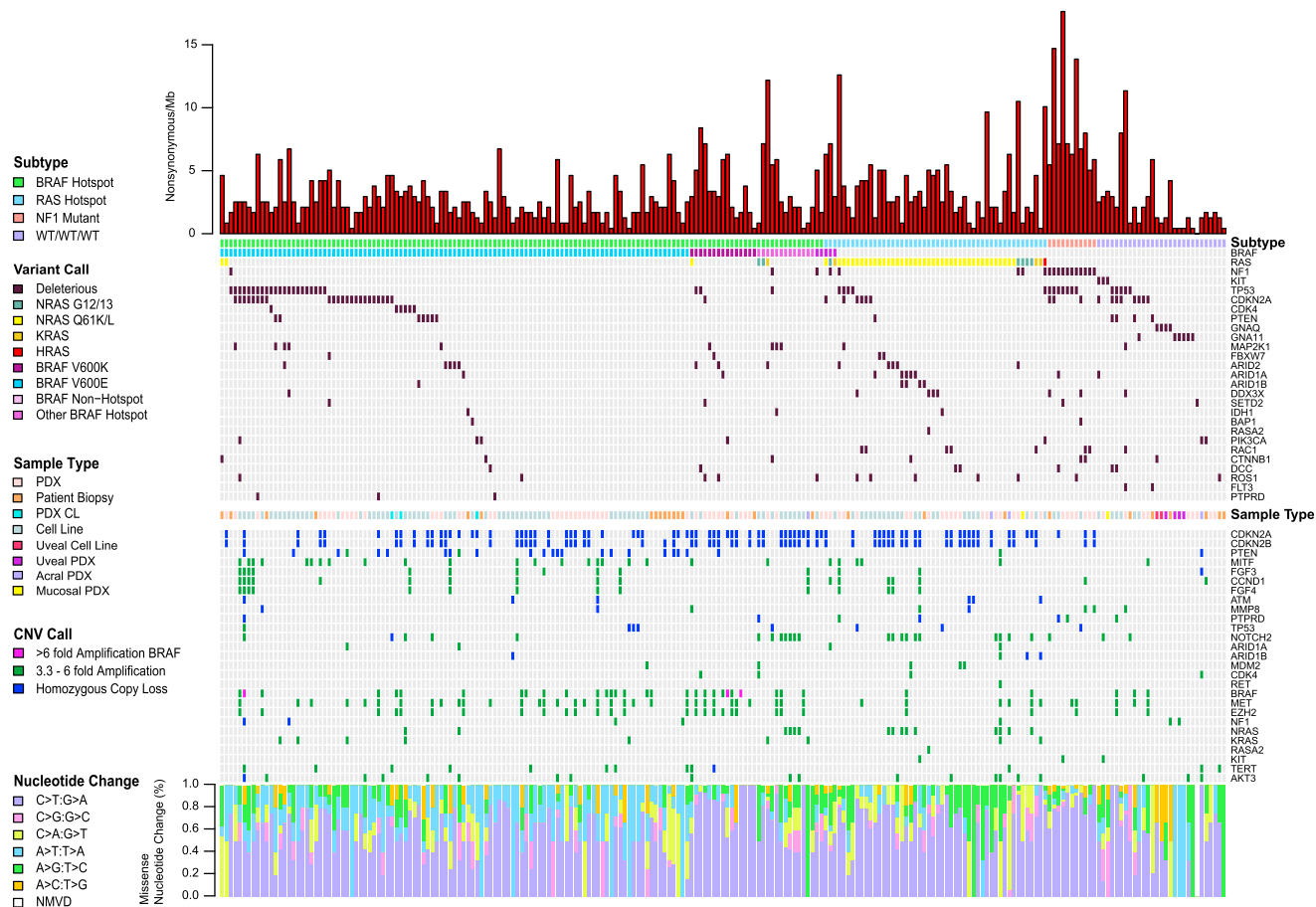


Figure 2. Mutational and Copy Number Profile of Naive Melanoma Cell Lines, PDXs, PDX CLs, and Tumors

A single sample from each of 225 unique patients is included. NMVD, no missense variants in targeted genes detected.

high-amplification events in *NOTCH2* co-occurred with high amplification in *NRAS*; both are on 1p. Of note, WT/WT/WT patients harbored significantly lower numbers of CNAs compared to hotspot *BRAF* and *RAS* subtypes ($p < 1 \times 10^{-4}$), but not to *NF1*-mutated samples.

We performed formal correlation analyses to examine co-occurrence of copy number changes that were found in more than 10% of samples (Figures S6B and S6C). When all samples were considered, significant correlations were identified between co-localized genes, such as deletion of *CDKN2A/CDKN2B* (9p21.3) and amplifications of *PREX2/SNX31/MYC* (8q) and *BRAF/RAC1/EGFR/EZH2/GRM3/DYNC111/CDK6/MET* (chr 7). Significant correlations between non-co-localized genes also were observed, with the most significant being between *MITF* amplification and *CDKN2A* deletion ($p = 0.0005$), *MITF* and *EGFR* amplifications ($p = 0.0005$), and *STK19* and *AKT3* amplifications ($p = 2 \times 10^{-5}$) (Figure S6B). The first two correlations are due to co-enrichment in *BRAF*-mutated samples. Within the *BRAF* mutant subset, the only correlation that emerged was between *MYC* and *STK19* amplifications ($p = 0.0001$) (Figure S6C). Little is known about *STK19* in melanoma; these data suggest further functional evaluation is warranted.

Genetic Landscape of Melanoma Cell Lines, PDXs, PDX CLs, and Patient Tumors Exposed to Targeted Therapies

Forty-nine (54 samples) unique patients had samples taken either post-progression (37) or on treatment (12) with targeted therapy; 21 (43%) were treated with a combination of BRAFi and MEKi, 27 (55%) BRAFi alone, and one MEKi alone (Figure 3A). Post-progression PDXs were expanded *in vivo* on a continuous BRAFi or BRAFi/MEKi to maintain the resistance phenotype (Krepler et al., 2016). Twenty (41%) patients received a combination of targeted and immunotherapy.

Potential resistance mechanisms were identified for 29 of 36 (81%) patients that progressed on treatment (Figure 3B) and classified into four categories: *BRAF* high-level amplifications (10, 28%), *NRAS* mutant (6, 17%), *MAP2K1* mutant (p.C121S, p.K57E/N, p.P124S, and p.Q56P) (7, 19%), and non-MAPK pathway alterations (*MITF* and *MET* high amplification and *PTEN* homozygous loss) (5, 14%). Although no deleterious mutations in *MAP2K2* were identified, a VUS (p.K61E) was found in the non-MAPK pathway-altered group, which may be associated with resistance. *MAP2K2* p.K61E has been reported in a patient with cardio-facio-cutaneous syndrome, one of the Rasopathies, supporting a functional role (Dentici et al., 2009).

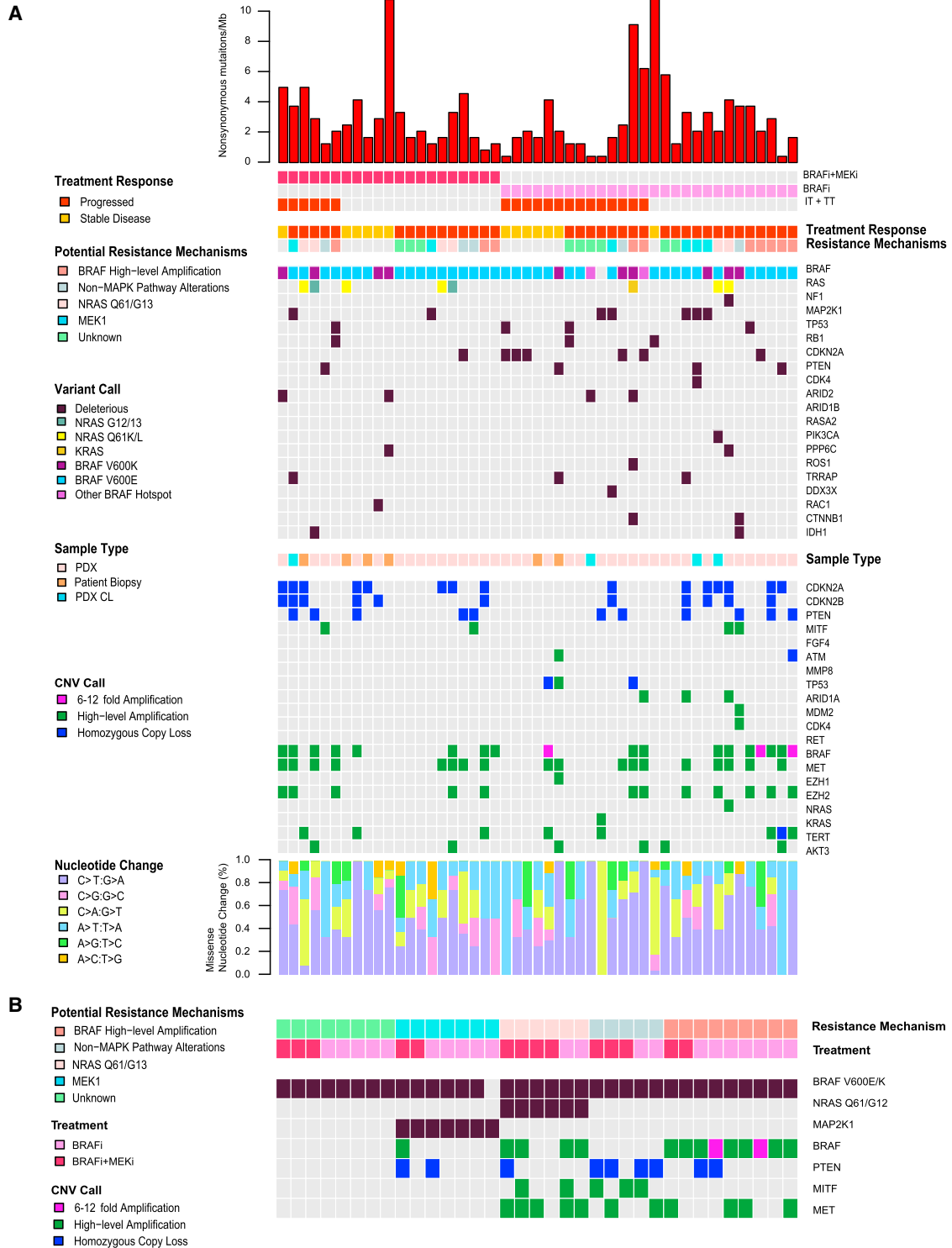


Figure 3. Mutational and Copy Number Profile of PDXs, PDX CLs, and Tumors from Patients that Received Targeted Therapy with BRAFi, MEKi, or a Combination

(A) A single sample from each of 49 unique patients is included.

(B) Five subtypes of potential resistance mechanisms in samples that progressed post-treatment.

Additional genetic and genomic changes were observed that also may contribute to therapeutic resistance (Figure 3B). Homozygous loss of *PTEN* and high-level amplification of *MET* were seen in 20% and 50% of patients with high-level amplification of *BRAF*, respectively. High-level amplification of *BRAF* was observed in 67% of samples also having secondary *NRAS* Q61/G12 mutations, along with additional CNAs in non-MAPK pathway genes. The mechanisms of resistance found in the samples did not differ between patients treated with BRAFi alone and with BRAFi/MEKi.

Genetic Landscape of Melanoma Cell Lines, PDXs, PDX CLs, and Patient Tumors from Patients Treated with Immunotherapy

Overall, 71 unique patients (two acral) were previously exposed to immunotherapy with anti-CTLA4 (33, 46%), anti-PD-1 (19, 27%), or anti-CTLA4/anti-PD1 (19, 27%). Twenty patients (28%) received both immunotherapy and targeted therapy. Of the 71 patients, eight (11%) patients were responders (one acral), 33 (47%) had progressive disease, seven (10%) had stable disease, and one patient (1%) had a mixed response (Figure 4). Disease outcome was unknown for 22 (31%) patients (one acral). The genetic and genomic landscape was similar to the naive sample set, with an enrichment for non-*BRAF*-mutated tumors. However, mutational burden (nonsynonymous variants/mb) in patients that received immunotherapy was significantly higher than the naive cohort ($p = 0.03$).

Evaluation of Multiple Samples from the Same Patient

Multiple samples from 40 patients were sequenced, including cell lines, PDXs, PDX CLs, and biopsies (Figure S7; Table S7). Full mutational concordance was observed across 65 samples from 28 (70%) patients; 35 samples from 12 patients were discordant. In six instances, discordance could be attributed to within-patient tumor heterogeneity, three instances to within-tumor heterogeneity, one instance to the development of acquired resistance mutations, two to acquired resistance mutations in cell lines adapting to targeted therapy, and in two instances no potential etiology could be identified. Discordant deleterious mutations in *KRAS* (p.A146T and p.K117N), *PTEN*, and *TACC1* were found in two biopsies taken on the same day but from different locations in a patient progressing on pembrolizumab/dabrafenib (WM4420). One patient had a total of five biopsies at three different time points; discordant mutations were observed in three genes, varying over time (before and after treatment with ipilimumab) and location (WM4295). We also observed discordant mutations in five genes in biopsies taken from left and right axillary lymph node metastases (WM4413). Further, an early-in-transit metastasis was found to have a deleterious *TP53* mutation, with two subsequent biopsies from different locations, while the patient was on BRAFi therapy for 12 months, both *TP53* WT (WM4011). Interestingly, the thick primary melanoma differed remarkably from a residual lung metastasis after anti-CTLA4 therapy (WM4210). We also observed two instances in which tumor grafts from the same PDX expanded in different mice did not have the same mutational changes.

These data suggest that intra-tumoral heterogeneity can lead to the outgrowth of several sub-clones during the propagation of

PDX, and they may explain some of the heterogeneity seen in PDX efficacy studies (Krepler et al., 2016). Therapeutic pressures also can lead to new mutations conferring selective growth advantages. In the *BRAF* V600E mutant model WM4351, two PDXs derived from therapy-naïve biopsies were both *NRAS* WT, whereas a biopsy taken after progression on BRAFi/MEKi had an *NRAS* Q61K mutation. In two cases, PDXs derived from targeted therapy-progressed patients did not demonstrate any acquired mutations, but they were resistant to the same therapy the patient had received when dosed *in vivo*. When we established cell line cultures, they initially did not grow, but they became resistant after several passages. Each cell line had a resistance mutation, one in *NRAS* (Q61K allele frequency 0.44) and the other in *MAP2K1* (C121S allele frequency 0.43) (Table S7).

Chromatin-Remodeling Gene Mutations in Melanoma Cell Lines, PDXs, PDX CLs, and Patient Tumors

Mutations in the genes that encode the SWI/SNF chromatin-remodeling enzymes *ARID1A* (BAF250A/SMARCF1), *ARID1B* (BAF250B), *ARID2* (BAF200), and *SMARCA4* (BRG1) have been implicated in melanoma, as have those that encode other chromatin organization/histone modification proteins (*EZH1*, *EZH2*, *SETD2*, and *TRRAP*) (Hodis et al., 2012; Cancer Genome Atlas Network, 2015). Overall, 65 of 371 (17.5%) samples from unique patients harbored a likely deleterious/deleterious mutation in at least one of the genes associated with chromatin remodeling or chromatin organization/histone modification (Figure 5). The most frequently mutated were *ARID2* (23), followed by *ARID1A* (13), *ARID1B* (7), and *SMARCA4* (4). Deleterious mutations in *ARID2*, *ARID1A*, and *SMARCA4* were mutually exclusive ($p = 2.2 \times 10^{-16}$), apart from a co-occurrence of *ARID2* and *SMARCA4* in one sample. However, deleterious mutations in *ARID1B* were found concurrently with mutations in *ARID2* (1) and *ARID1A* (2). Restricting to naive samples to reduce bias, *BRAF* V600E mutations were the least likely to be associated with chromatin-remodeling gene mutations (7 of 105, 7%). Chromatin-remodeling gene mutations were observed comparatively frequently with *BRAF* V600K (3 of 15, 20%), *RAS* (12 of 50, 24%), and *NF1* (1 of 11, 9%) mutations ($p = 0.013$). One deleterious truncating mutation was detected in *EZH1*; deleterious/likely deleterious missense mutations were found in 12 *EZH1/2*-mutated samples from unique patients. Rare mutually exclusive mutations were found in *SETD2* (4), *TRRAP* (4), *IDH1* (1), and *BAP1* (1).

Comparison of Genotypes in Clinical Samples and PDXs

Clinical tumor sequencing data from 79 melanoma patients treated at Penn Medicine or MDACC were compared to our data (Table 2). At the Center for Personalized Diagnostics at Penn Medicine, the TruSeq Amplicon Cancer Panel (Illumina) was used for clinical sequencing (Hiemenz et al., 2016). At MDACC, CMS50 (Life Technologies) was used for clinical sequencing (Kim et al., 2017). For each patient, mutational profiles of PDX or tumor biopsy were compared to the clinical mutational profile. It is important to note that, in virtually all cases, a different sample was used for clinical sequencing than to establish the PDX or sent as a research tumor biopsy.

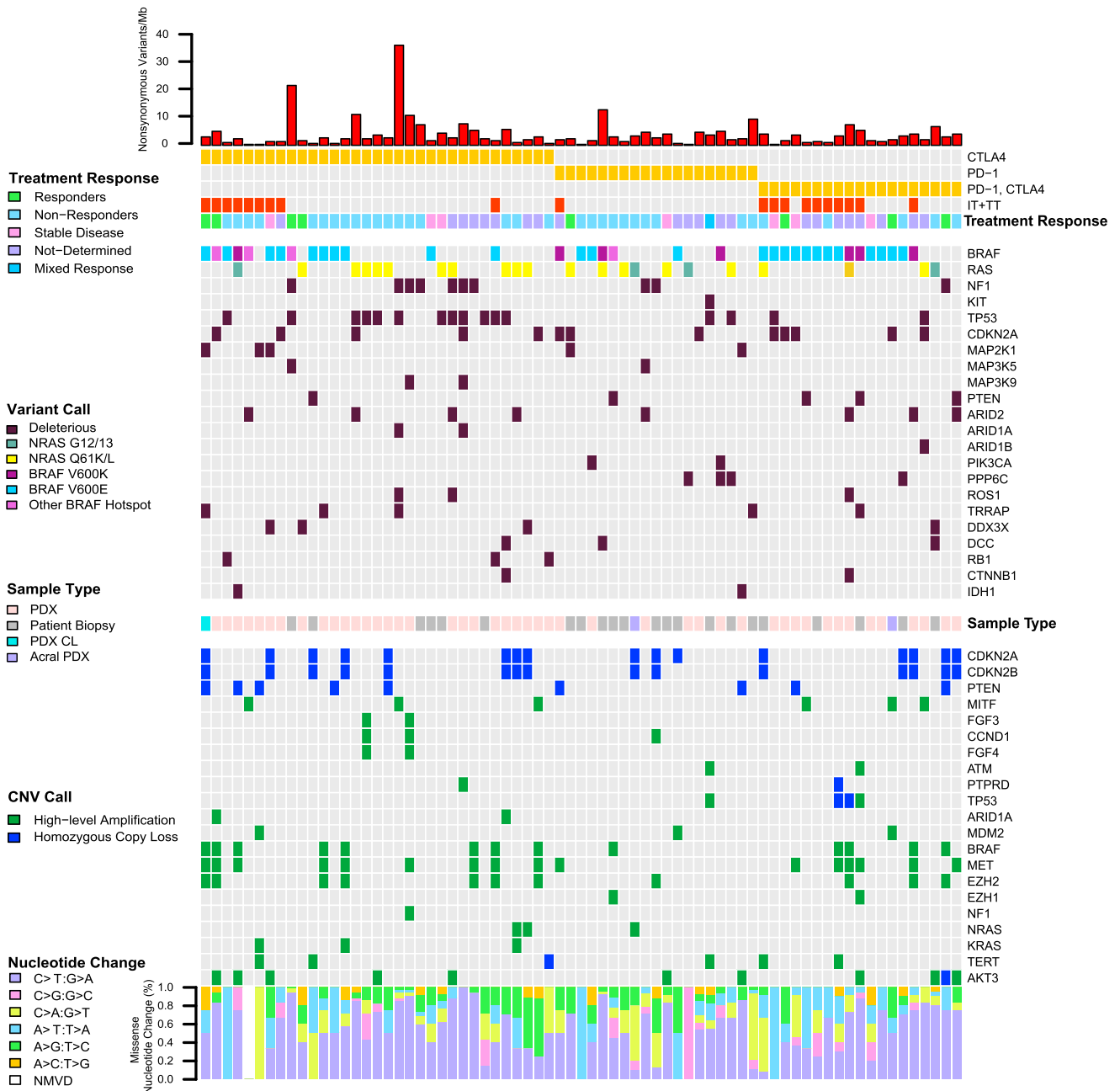


Figure 4. Mutational and Copy Number Profile of PDXs, PDX CLs, and Tumors from Patients that Received Immunotherapy with Anti-CTLA-4, Anti PD-1, or a Combination

A single sample from each of 49 unique patients is included. NMVD, no missense variants in targeted genes detected.

Additionally, we could only compare samples for which positive results were found on either clinical or study sequencing in regions covered by both. All deleterious mutations were determined to be such by both the site and study. However, for six likely deleterious mutations and VUSs, the pathogenicity calls varied.

Overall, there were 101 potentially overlapping mutations, of which 91 (91%) were found by both the site and study. We iden-

tified eight of 63 (12.6%) samples with discordant results. Of those, four (WM3407, WM4428, WM4462, and WM4464) research biopsies were likely normal tissue rather than melanoma, as they had one to three VUSs at allelic frequencies of 50%. For two samples (WM4433 and WM4323), although clinical sequencing was done on a pre-treatment sample, we sequenced a post-treatment sample and identified presumably *de novo* resistance mutations. In one sample (WM4279), we

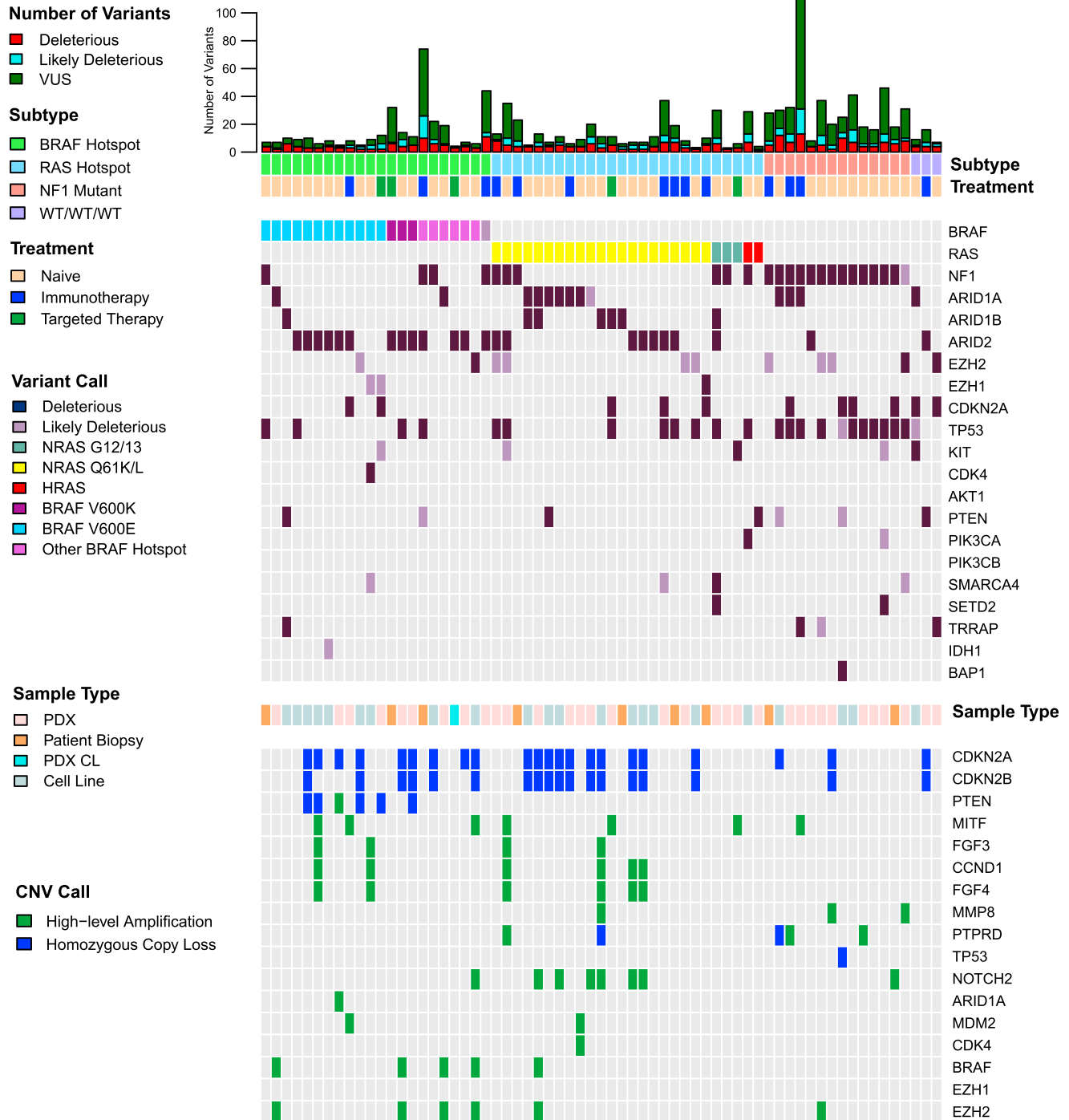


Figure 5. Mutational and Copy Number Profile in Unique Patient Cell Lines and PDXs with a Likely Deleterious/Deleterious Mutation in Chromatin-Remodeling Genes, which Reveals Mutual Exclusivity of Mutations

identified a *KIT* p.L576P mutation not found in the clinical samples. Of the 16 UPENN samples with sequencing of a clinical sample and PDX, we only found one (6%) with discrepant results; interestingly, we each found different truncating mutations in *PTEN*. We observed that mutations tended to have higher

allele frequencies in the PDX, as compared to clinical sequencing, which could be due to either admixture in the original tumor or loss of the wild-type allele during establishment of the PDX, which we have observed for ovarian cancer PDX (George et al., 2017).

Table 2. Results from Clinical and Study Sequencing of Samples from the Same Patient

Sample ID	Sample Type	Clinical Site	Gene	NT Change	Site Variant Call	Study Variant Call	Percentage Tumor	Tumor AF (%)	PDX AF (%)	Percentage Increase	Concordance
WM4428	patient biopsy	MDACC	<i>BRAF</i>	c.T1799A:p.V600E	deleterious	–	–	–	–	–	discordant
WM4433	patient biopsy	MDACC	<i>BRAF</i>	c.T1799A:p.V600E	deleterious	deleterious	–	22.6	–	–	concordant
WM4433	patient biopsy	MDACC	<i>NRAS</i>	c.A182G:p.Q61R	–	deleterious	–	32.5	–	–	discordant
WM4435	patient biopsy	MDACC	<i>BRAF</i>	c.T1799A:p.V600E	deleterious	deleterious	–	28.4	–	–	concordant
WM4437	patient biopsy	MDACC	<i>BRAF</i>	c.GT1798_1799AA:p.V600K	deleterious	deleterious	–	33.7	–	–	concordant
WM4444	patient biopsy	MDACC	<i>BRAF</i>	c.GT1798_1799AA:p.V600K	deleterious	deleterious	–	90	–	–	concordant
WM4449	patient biopsy	MDACC	<i>BRAF</i>	c.T1799A:p.V600E	deleterious	deleterious	–	56.9	–	–	concordant
WM4462	patient biopsy	MDACC	<i>BRAF</i>	c.T1799A:p.V600E	deleterious	–	–	–	–	–	discordant
WM4464	patient biopsy	MDACC	<i>BRAF</i>	c.T1790G:p.L597R	deleterious	–	–	–	–	–	discordant
WM4472	patient biopsy	MDACC	<i>BRAF</i>	c.T1799A:p.V600E	deleterious	deleterious	–	44.3	–	–	concordant
WM4478	patient biopsy	MDACC	<i>BRAF</i>	c.A1801G:p.K601E	deleterious	deleterious	–	42.4	–	–	concordant
WM4487	patient biopsy	MDACC	<i>BRAF</i>	c.T1799A:p.V600E	deleterious	deleterious	–	52.1	–	–	concordant
WM4494	patient biopsy	MDACC	<i>BRAF</i>	c.GT1798_1799AA:p.V600K	deleterious	deleterious	–	29.2	–	–	concordant
WM4500	patient biopsy	MDACC	<i>BRAF</i>	c.T1799A:p.V600E	deleterious	deleterious	–	53.8	–	–	concordant
WM4508	patient biopsy	MDACC	<i>BRAF</i>	c.1799_1801del:p.600_601del	deleterious	deleterious	–	36.4	–	–	concordant
WM4515	patient biopsy	MDACC	<i>NRAS</i>	c.A182G:p.Q61R	deleterious	deleterious	–	50.8	–	–	concordant
WM4528	patient biopsy	MDACC	<i>NRAS</i>	c.C181A:p.Q61K	deleterious	deleterious	–	41.8	–	–	concordant
WM4530	patient biopsy	MDACC	<i>NRAS</i>	c.A182G:p.Q61R	deleterious	deleterious	–	48	–	–	concordant
WM4532	patient biopsy	MDACC	<i>BRAF</i>	c.T1799A:p.V600E	deleterious	deleterious	–	47.5	–	–	concordant
WM4542	patient biopsy	MDACC	<i>NRAS</i>	c.A182G:p.Q61R	deleterious	deleterious	–	46.2	–	–	concordant
WM4545	patient biopsy	MDACC	<i>BRAF</i>	c.T1799A:p.V600E	deleterious	deleterious	–	44.6	–	–	concordant
WM4553	patient biopsy	MDACC	<i>BRAF</i>	c.T1799A:p.V600E	deleterious	deleterious	–	49.4	–	–	concordant
WM4558	patient biopsy	MDACC	<i>BRAF</i>	c.T1799A:p.V600E	deleterious	deleterious	–	47.7	–	–	concordant
WM3407	PDX	MDACC	<i>BRAF</i>	c.G1397A:G466E	deleterious	ND	–	–	–	–	discordant
WM3407	PDX	MDACC	<i>ATM</i>	c.T728C:p.L243S	VUS‡	VUS	–	48.1	–	–	concordant
WM4218	PDX	MDACC	<i>KIT</i>	c.T1669C:p.W557R	deleterious	deleterious	–	47.1	–	–	concordant
WM4249	PDX	MDACC	<i>BRAF</i>	c.T1799A:p.V600E	deleterious	deleterious	–	61.7	–	–	concordant
WM4257	PDX	MDACC	<i>NRAS</i>	c.C181A:p.Q61K	deleterious	deleterious	–	75	–	–	concordant
WM4257	PDX	MDACC	<i>TP53</i>	c.G629A:p.R210K	deleterious	deleterious	–	100	–	–	concordant
WM4258	PDX	MDACC	<i>BRAF</i>	c.T1799A:p.V600E	deleterious	deleterious	–	48.1	–	–	concordant
WM4260	PDX	MDACC	<i>KIT</i>	c.A1924G:p.K642E	deleterious	deleterious	–	78.3	–	–	concordant
WM4260	PDX	MDACC	<i>CTNNB1</i>	c.C134T:p.S45F	deleterious	deleterious	–	49.9	–	–	concordant
WM4262	PDX	MDACC	<i>BRAF</i>	c.T1799A:p.V600E	deleterious	deleterious	–	99.8	–	–	concordant
WM4264	PDX	MDACC	<i>BRAF</i>	c.T1799A:p.V600E	deleterious	deleterious	–	64.7	–	–	concordant
WM4265-1	PDX	MDACC	<i>NRAS</i>	c.C181A:p.Q61K	deleterious	deleterious	–	96.8	–	–	concordant
WM4265-1	PDX	MDACC	<i>TP53</i>	c.C380T:p.S127F	deleterious	deleterious	–	98	–	–	concordant

(Continued on next page)

Table 2. Continued

Sample ID	Sample Type	Clinical Site	Gene	NT Change	Site Variant Call	Study Variant Call	Percentage Tumor	Tumor AF (%)	PDX AF (%)	Percentage Increase	Concordance
WM4267	PDX	MDACC	<i>BRAF</i>	c.T1799A:p.V600E	deleterious	ND			–		discordant
WM4267	PDX	MDACC	<i>CDKN2A</i>	c.G159C:p.M53I	VUS	VUS			55.1		concordant
WM4276	PDX	MDACC	<i>BRAF</i>	c.T1799A:p.V600E	deleterious	deleterious			0.61		concordant
WM4279	PDX	MDACC	<i>KIT</i>	c.T1727C:p.L576P	ND	deleterious			86.6		discordant
WM4280	PDX	MDACC	<i>BRAF</i>	c.GT1798_1799AA:p.V600K	deleterious	deleterious			47.6		concordant
WM4285	PDX	MDACC	<i>BRAF</i>	c.T1799A:p.V600E	deleterious	deleterious			42.2		concordant
WM4286-1	PDX	MDACC	<i>BRAF</i>	c.T1799A:p.V600E	deleterious	deleterious			0.59		concordant
WM4292	PDX	MDACC	<i>BRAF</i>	c.T1799A:p.V600E	deleterious	deleterious			48.6		concordant
WM4295	PDX	MDACC	<i>NRAS</i>	c.A182T:p.Q61L	deleterious	deleterious			96.3		concordant
WM4299-1	PDX	MDACC	<i>NRAS</i>	c.A182T:p.Q61L	deleterious	deleterious			0.93		concordant
WM4306	PDX	MDACC	<i>BRAF</i>	c.T1799A:p.V600E	deleterious	deleterious			25.2		concordant
WM4323	PDX	MDACC	<i>BRAF</i>	c.T1799A:p.V600E	deleterious	–			–		discordant
WM4323	PDX	MDACC	<i>MAP2K1</i>	c.1029dupA:p.I343fs	NC†	deleterious			46.2		discordant
WM4335	PDX	MDACC	<i>BRAF</i>	c.T1799A:p.V600E	deleterious	deleterious			28.7		concordant
WM4345	PDX	MDACC	<i>BRAF</i>	c.T1799A:p.V600E	deleterious	deleterious			61		concordant
WM4345	PDX	MDACC	<i>CDKN2A</i>	c.C238T:p.R80X	deleterious	deleterious			84		concordant
WM4351	PDX	MDACC	<i>BRAF</i>	c.T1799A:p.V600E	deleterious	deleterious			75.5		concordant
WM4353	PDX	MDACC	<i>BRAF</i>	c.T1799A:p.V600E	deleterious	deleterious			57		concordant
WM4367	PDX	MDACC	<i>BRAF</i>	c.T1799A:p.V600E	deleterious	deleterious			51.2		concordant
WM4369	PDX	MDACC	<i>NRAS</i>	c.G38A:p.G13D	deleterious	deleterious			65.6		concordant
WM4370	PDX	MDACC	<i>BRAF</i>	c.GT1798_1799AA:p.V600K	deleterious	deleterious			92.7		concordant
WM4380	PDX	MDACC	<i>BRAF</i>	c.T1799A:p.V600E	deleterious	deleterious			30.7		concordant
WM4382	PDX	MDACC	<i>BRAF</i>	c.T1799A:p.V600E	deleterious	deleterious			48.6		concordant
WM4388	PDX	MDACC	<i>BRAF</i>	c.T1799A:p.V600E	deleterious	deleterious			47		concordant
WM4388	PDX	MDACC	<i>TP53</i>	c.C520T:p.R174X	deleterious	deleterious			91.3		concordant
WM4389	PDX	MDACC	<i>NRAS</i>	c.G37C:p.G13R	deleterious	deleterious			73.1		concordant
WM4404	PDX	MDACC	<i>BRAF</i>	c.T1799A:p.V600E	deleterious	deleterious			67.7		concordant
WM4408	PDX	MDACC	<i>BRAF</i>	c.T1799A:p.V600E	deleterious	deleterious			74.1		concordant
WM4420	PDX	MDACC	<i>BRAF</i>	c.GT1798_1799AA:p.V600K	deleterious	deleterious			87.7		concordant
WM4420	PDX	MDACC	<i>CTNNB1</i>	c.C134T:p.S45F	deleterious	deleterious			65		concordant
WM4420	PDX	MDACC	<i>FBXW7</i>	c.C1321T:p.R441W	deleterious	deleterious			52.6		concordant
WM4426	PDX	MDACC	<i>NRAS</i>	c.A182G:p.Q61R	deleterious	deleterious			84.5		concordant
WM4430	PDX	MDACC	<i>NRAS</i>	c.A182G:p.Q61R	deleterious	deleterious			100		concordant
WM4442	PDX	MDACC	<i>NRAS</i>	c.C181A:p.Q61K	deleterious	deleterious			95.7		concordant
WM4445	PDX	MDACC	<i>BRAF</i>	c.T1799A:p.V600E	deleterious	deleterious			56.7		concordant
WM4451	PDX	MDACC	<i>NRAS</i>	c.G35A:p.G12D	deleterious	deleterious			87.4		concordant

(Continued on next page)

Table 2. Continued

Sample ID	Sample Type	Clinical Site	Gene	NT Change	Site Variant Call	Study Variant Call	Percentage Tumor	Tumor AF (%)	PDX AF (%)	Percentage Increase	Concordance
WM4454	PDX	MDACC	<i>TP53</i>	c.T708G;p.C236W	deleterious	deleterious			100		concordant
WM4454	PDX	MDACC	<i>BRAF</i>	c.T1799A;p.V600E	deleterious	deleterious			45.3		concordant
WM4465	PDX	MDACC	<i>BRAF</i>	c.GT1798_1799AA;p.V600K	deleterious	deleterious			29.2		concordant
WM3901	PDX	UPENN	<i>BRAF</i>	c.T1799A;p.V600E	deleterious	deleterious	44	67.05	84.9	26.6	concordant
WM4011	PDX	UPENN	<i>BRAF</i>	c.GT1798_1799AA;p.V600K	deleterious	deleterious	26–50	13.82	76.6	454.3	concordant
WM4042	PDX	UPENN	<i>NRAS</i>	c.A182G;p.Q61R	deleterious	deleterious	>50	34.26	98.9	188.7	concordant
WM4068	PDX	UPENN	<i>BRAF</i>	c.G1406A;p.G469E	deleterious	deleterious	>50	35	47	34.2	concordant
WM4068	PDX	UPENN	<i>KRAS</i>	c.G35A;p.G12D	deleterious	deleterious	>50	61.1	73.7	20.6	concordant
WM4206	PDX	UPENN	<i>BRAF</i>	c.GT1798_1799AA;p.V600K	deleterious	deleterious	>50	35.06	65.6	87.1	concordant
WM4208	PDX	UPENN	<i>NRAS</i>	c.A182G;p.Q61R	deleterious	deleterious	>50	19.13	64	234.6	concordant
WM4224	PDX	UPENN	<i>NRAS</i>	c.A182G;p.Q61R	deleterious	deleterious	44	10.14	47.7	370.4	concordant
WM4224	PDX	UPENN	<i>TP53</i>	c.C211T;p.R71C	deleterious	deleterious	44	12.03	57.6	378.8	concordant
WM4224	PDX	UPENN	<i>CTNNB1</i>	c.A121G;p.T41A	deleterious	deleterious	44	28.5	98.8	246.7	concordant
WM4231	PDX	UPENN	<i>RET</i>	c.C2672T;p.S891L	VUS	likely deleterious	>50	25.68	50.2	95.5	concordant
WM4231	PDX	UPENN	<i>NRAS</i>	c.A182G;p.Q61R	deleterious	deleterious	>50	30.25	52.5	73.6	concordant
WM4237	PDX	UPENN	<i>RB1</i>	c.2069_2082del;p.N690fs	deleterious	deleterious	26–50	38.41	73.8	92.1	concordant
WM4237	PDX	UPENN	<i>BRAF</i>	c.T1799A;p.V600E	deleterious	deleterious	26–50	21.21	76.3	259.7	concordant
WM4237	PDX	UPENN	<i>TP53</i>	c.C722T;p.S241F	deleterious	deleterious	26–50	40.62	99.2	144.2	concordant
WM4240	PDX	UPENN	<i>SMAD4</i>	c.G1399C;p.G467R	VUS	likely deleterious	100	43.33	41.7	–	concordant
WM4243	PDX	UPENN	<i>BRAF</i>	c.T1799A;p.V600E	deleterious	deleterious	>50	41.06	50.1	22.0	concordant
WM4298	PDX	UPENN	<i>KIT</i>	c.T1688A;p.I563K	likely deleterious	VUS	>50	61.05	98	60.5	concordant
WM4298	PDX	UPENN	<i>BRAF</i>	c.T1799A;p.V600E	deleterious	deleterious	>50	50.9	98.8	94.1	concordant
WM4314	PDX	UPENN	<i>FGFR2</i>	c.811_812delinsAA;p.G271K	likely deleterious	likely deleterious	>50	34.96	46.2	–	discordant
WM4349	PDX	UPENN	<i>BRAF</i>	c.T1799A;p.V600E	deleterious	deleterious	26–50	24.63	51.8	110.3	concordant
WM4364	PDX	UPENN	<i>BRAF</i>	c.T1799A;p.V600E	deleterious	deleterious	>50	42.91	55.6	29.6	concordant
WM4364	PDX	UPENN	<i>PTEN</i>	c.208_209+1del	deleterious	ND	>50	72.59	ND	–	discordant
WM4364	PDX	UPENN	<i>PTEN</i>	c.727_728del;p.L243fs	ND	deleterious	>50	ND	78.5	–	discordant
WM4543	PDX	UPENN	<i>KDR</i>	c.G4066T;p.V1356F	VUS	VUS	26–50	6.84	44	543.3	concordant
WM4543	PDX	UPENN	<i>BRAF</i>	c.T1799A;p.V600E	deleterious	deleterious	26–50	6.4	40.4	531.3	concordant

ND, not detected; NC, not captured; VUS, variant of uncertain significance.

DISCUSSION

In this era of precision medicine, pre-clinical drug development of targeted oncology therapeutics relies heavily on models of cancer that have been shown to be representative of the genetic profile of the patient's tumor. Herein, we demonstrate that targeted massively parallel sequencing of 108/119 genes previously implicated in melanomagenesis, followed by our custom analysis pipelines for mutational and CNV calling, is a reliable method for characterizing the genetic and genomic landscape of melanoma cell lines, tumors, PDXs, and PDX CLs. To account for the lack of matched normal samples, control samples were sequenced in each lane for normalization for copy number calling and to identify common variants, which were subtracted out. We also removed sequences that more closely aligned to the mouse than human genome to decrease cross-contamination and increase accuracy of mutational and copy number calling. We used an in-house-developed pipeline to classify mutations or variants as deleterious, likely deleterious, and VUS, incorporating information from the literature and Catalogue of Somatic Mutations in Cancer (COSMIC), mutational type, location, and effect, after filtering for a maximum population frequency greater than or equal to 0.1% to account for the lack of a matched normal.

We found the total number of mutation and variant calls did not differ significantly among cell lines, PDXs, PDX CLs, and patient tumors, although, not surprisingly, there was a trend toward higher mutational rates in PDXs and cell lines. We observed significantly higher rates of *BRAF* and *RAS* mutations and *CDKN2A* mutations/loss in cell lines than PDXs and tumor biopsies, consistent with the growth advantage conferred by those mutations. However, we did find cell lines representing all mutational groups. We also found an extremely high concordance rate between clinical sequencing results and our targeted sequencing, with only two samples of 80 (2.5%) demonstrating truly discrepant results. Taken together, the mutational profiles observed in the melanoma cell lines, PDXs, and PDX CLs sequenced in this study are an accurate genetic and genomic representation of the patient's original tumor. We also identified all major previously reported melanoma subtypes, as well as the full spectrum of mutations and copy number aberrations, at roughly the same frequencies identified in large-scale original patient tumor/normal sequencing studies (Berger et al., 2012; Hodis et al., 2012; Krauthammer et al., 2015; Cancer Genome Atlas Network, 2015). Thus, we have a unique genetically and genomically annotated biobank of PDXs, PDX CLs, and cell lines, representative of the full spectrum of melanoma, which can be used both for functional studies and pre-clinical drug development studies in melanoma.

Our large sample set also enabled us to describe rare subtypes in greater detail. We found two mutually exclusive patterns of mutations in the MAPK-signaling pathway: (1) single-hotspot mutations at *BRAF* V600 or *NRAS* Q61; and (2) multiple non-hotspot variants across different genes encoding proteins within the MAPK-signaling pathway, of which *NF1* mutations are a subset. All deleterious/likely deleterious non-600 mutations in *BRAF*, 87% of the *NF1*, 75% of the non-Q61 *RAS*, and 44% of *KIT* mutant samples harbored either a secondary mutation or high-

level amplification in at least one gene encoding a MAPK-signaling protein or an effector protein of the MAPK pathway. These data are consistent with functional studies that have demonstrated that kinase-dead *BRAF* (D594 mutants) needs oncogenic *RAS* to drive tumor progression (Heidorn et al., 2010). Our results also suggest that *BRAF* mutations (e.g., at G464 and G469) leading to constitutive dimerization (Yao et al., 2015) also need at least one additional MAPK-signaling mutation to drive tumor progression, either a single *NRAS* G12/13 or multiple other mutations. These data suggest that, to accurately characterize therapeutic response pre-clinically for non-V600 *BRAF* or non-Q61 *NRAS* mutations, a second MAPK-signaling mutation will be needed to be included in the model. Further, we can make predictions about the functionality of uncharacterized *BRAF* non-V600 mutations, in that if the alteration is found without a secondary MAPK-signaling pathway gene mutation or in the presence of a *BRAF* V600 gene mutation, it is very unlikely to have any functional significance. Similar to *BRAF* non-V600 mutations, *RAS* G12/13 mutations usually are observed with co-occurring mutations, most commonly in *BRAF* and *NF1*, suggesting they are not sufficient to drive tumorigenesis in melanoma, in contrast to other tumor types (Hobbs et al., 2016).

We identified additional MAPK pathway or co-activating gene mutations in 87% of *NF1* mutant tumors. We did not observe any difference between those with one or two truncating *NF1* mutations or with accompanying loss of the wild-type allele. Prior literature has suggested an enrichment for co-occurring mutations in Rasopathy genes, particularly *PTPN11* and *RASA2* (Arafah et al., 2015; Cirenajwis et al., 2017; Krauthammer et al., 2015). However, we observed co-occurrence of deleterious mutations across numerous genes without specific enrichment, including those that have not been previously implicated as co-mutated with *NF1*, although known to be mutated in melanoma, *MAP3K5* and *MAP3K9*. Functional studies of *BRAF^{wt}/RAS^{wt}* melanoma cell lines lacking *NF1* expression, or expressing *NF1* at extremely low levels, have shown that not all have *RAS* activation and that only some were sensitive to MEKi (Krauthammer et al., 2015). This result may be explained by the co-occurrence of other MAPK-signaling gene mutations. Pre-clinical modeling of response to therapies for *NF1*-mutated melanoma also will need to account for co-occurring mutations. The *NF1* mutant cohort harboring co-mutations in *MAP3K5/9* is of particular interest, as they are upstream activators of the Jun N-terminal kinase (JNK) and p38 MAPK pathways (Rana et al., 2013). The current study provides the reagents to further functionally characterize this interesting rare subtype of melanoma.

Although previous sequencing studies have identified *ARID1A/B*, *ARID2*, *IDH1*, *SMARCA4A*, *TRRAP*, and *EZH2* as chromatin-remodeling genes frequently mutated in melanoma (Berger et al., 2012; Hodis et al., 2012; Zhang et al., 2016), their mutual exclusivity has not been well described. Given this finding, it is likely that the previously described *ARID1B* dependence in *ARID1A*-mutated ovarian cancer cells (Helming et al., 2014) is recapitulated in melanoma, as well as the *EZH2* dependency in tumors with mutations in *ARID1A* or *SMARCA4* that do not harbor co-mutations in *RAS* or *BRAF* (Kim et al., 2015). However, a few *ARID1A*- and *SMARCA4*-mutated samples in our

dataset do have co-mutations in *BRAF* or *RAS*, which has been postulated to abolish *EZH2* dependency (Kim et al., 2015), so further investigation is needed. The biological relevance of the likely deleterious missense mutations we identified in *ARID1A/B* and *ARID2*, which occur alone and concurrently with other *ARID1A/B* and *EZH2* mutations, also needs to be evaluated functionally. Pre-clinical studies using these PDX models may reveal other specific vulnerabilities in melanomas, with a mutation in *SWI/SNF* components *ARID1A*, *ARID1B*, *ARID2*, or *SMARCA4A*, that will aid in the development of novel therapeutics.

We profiled 37 PDXs, PDX CLs, and tumor biopsies from patients that progressed on targeted therapy (either BRAFi or BRAFi/MEKi). Our evaluation for resistance mechanisms was limited by a lack of matched pre-treatment or normal samples and RNA to evaluate for splice variants or potential fusions. However, we identified mutations in *NRAS*, *MAP2K1*, and *BRAF* amplification at rates similar to other series (Johnson et al., 2015). Amplification of *BRAF* was enriched in this set (40%), as compared to the naive group (15%, $p = 2 \times 10^{-4}$). For the two PDXs with high-level *BRAF* amplifications, it likely is the primary mechanism of resistance. For other samples with *BRAF* amplification, it is a potential mechanism of resistance, but it cannot not be definitively proven as we lacked matched pre-treatment samples. For 51% of samples, we did not identify a clear mechanism of resistance; in half of those, we found amplifications and drivers outside the MAPK-signaling pathway that may be associated with resistance. We also profiled PDXs, PDX CLs, and tumor biopsies from 71 patients that had received checkpoint blockade therapy. The genetic and genomic landscape of these samples was similar to naive samples, albeit with increased mutational burden and enrichment for non-*BRAF* mutations. These post-treatment PDXs are ideal for further studies to identify potential resistance mechanisms and pre-clinical studies of potential therapeutics for tumors resistant to either targeted or checkpoint therapy.

Our study has several limitations, when compared to prior tumor-based analyses. Although the samples are derived from human tumors, they are established in culture or as PDX models in T cell-deficient (nude) mice, so they are not subject to an intact immune system, which may lead to differential selective pressures for mutations or copy number aberrations. Additionally, intra-tumor heterogeneity observed in PDX expansion (Tentler et al., 2012) can result in potentially inharmonious PDX/PDX CL and tumor mutational profiles. We observed a high consistency between clinical testing and our profiling, likely because the former mainly included major driver genes. However, when we sequenced multiple samples from the same individual, we found several instances of both within-patient and within-tumor heterogeneity. Further, several of the tumor biopsies (but neither PDXs nor cell lines) that we sequenced that fall into the WT/WT/WT group may be normal tissue, as histopathology was not done on these research samples. Platform and analytical differences also may lead to differences among mutational and copy number rates among studies. As we did not have a matched normal sequence for subtraction, we used population-based data, non-matched normal and stringent calling metrics to identify deleterious and likely deleterious mutations, but these are imper-

fect controls. We also chose to only report out high-level amplifications and homozygous deletions, to be conservative. Thus, for some genes, our data appear different than prior studies. For example, mutations in *GRIN2A* and *TRRAP* are reported in 22% and 12%, respectively, of melanomas in a meta-analysis of somatic mutations across studies (Zhang et al., 2016); but, since we classified most variants in these genes as VUSs, our reported rates of deleterious/likely deleterious mutations are much lower at 6% and 5.6%. Additionally, we are limited by the genes and regions included in our panel at the time of design, and so we have not interrogated recently identified recurrently mutated promoter regions, genes associated with resistance to checkpoint blockage, and the Rasopathy genes in all samples. Performing unbiased whole-exome or whole-genome sequencing on 462 samples was not possible due to cost restrictions.

This unparalleled biobank of melanoma cell lines, PDXs, and PDX CLs in this study provides a set of reagents for not only future melanoma drug discovery and development efforts but also extensive biological studies. We have characterized 146 cell lines (31 derived from PDXs), 248 PDXs, and 68 tumor biopsies, which include both those naive to treatment and resistant to targeted therapy and checkpoint blockade. We have been able to identify all major and minor subtypes of melanoma, thus providing reagents that, in some cases, were previously unavailable for functional and biological studies. Although further evaluation will need to be done in some instances to characterize the reagents (e.g., targeted therapy progression samples for which no mechanism of resistance was identified), the current genetic and genomic copy number data provide a strong basis for future studies. These reagents enable thoughtful pre-clinical trials to be designed to determine the *in vivo* efficacy of novel single-agent and combination therapies in genetically defined melanoma subsets, as demonstrated in the companion paper (Krepler et al., 2017).

EXPERIMENTAL PROCEDURES

Sample Acquisition

Acquisition of patient samples for the purposes of establishing PDXs and cell lines was approved by the corresponding institutions' institutional review boards, and informed consent was obtained from each participant for use of his or her sample in genetic studies. Tumors were provided from the following institutions: Perelman School of Medicine at the University of Pennsylvania, MD Anderson Cancer Center, Helen F. Graham Cancer Center, Massachusetts General Hospital, the John Wayne Cancer Institute, the Center for Melanoma and Cancer Immunotherapy at Hadassah Hebrew University Medical Center's Sharett Institute of Oncology, and the University of Duisburg-Essen.

A full description of PDX development is given in our companion paper (Krepler et al., 2016). As part of this study, 114 human melanoma cell lines, 246 PDXs, 60 PDX CLs, and 68 patient tumors were sequenced (total number of samples: 462) (Table S1). In addition to melanoma cell lines, PDXs, and PDX CLs, 36 unmatched anonymous germline blood samples were sequenced simultaneously, which were used for the normalization for copy number calling.

Processing of Sequencing Data

Short-read sequences were aligned to the GRCh37 human reference genome using the Burrows-Wheeler Aligner (BWA) (Li and Durbin, 2009). Duplicate reads were flagged, as well as reads that mapped equally to more than one location. Human reads were further disambiguated from mouse by aligning to the mm10 reference genome using the Python script

(<https://github.com/AstraZeneca-NGS/disambiguate>), which takes the human_aligned.bam and the mouse_aligned.bam as input. Reads that aligned more confidently to the mouse genome, as well as ambiguous reads between the two species, were discarded. To achieve acceptable data quality assurance, the Broad Institute's Genome Analysis Toolkit (GATK) "Best Practices" guidelines were followed. Single-nucleotide variant (SNV) and small insertion and deletion (indel) variant calling was performed by GATK UnifiedGenotyper (DePristo et al., 2011; McKenna et al., 2010), VarDict (Lai et al., 2016), and FreeBayes (Garrison and Marth, 2012). Variants with a read depth less than 20 and alternative allele read depth less than five, as well as all synonymous variants, and/or variants present in the germline samples, were excluded. However, variants that were called by more than one variant caller and had a sequencing depth of less than 20 were not excluded. Variants were annotated with a customized version of ANNOVAR (Wang et al., 2010). Variants were removed if the minor allele frequency was greater than or equal to 0.1% in the population databases 1000 Genomes (Abecasis et al., 2012) and/or Exome Aggregation Consortium (ExAC) (Lek et al., 2016) or found in normal germline samples sequenced on our capture. The remaining annotated variants were classified as outlined in Figure S1. Variant classification was confirmed with cBioPortal for Cancer Genomics, wherever possible (Cerami et al., 2012), and using ClinVar for the Rasopathy genes (<https://www.ncbi.nlm.nih.gov/clinvar>). Integrative Genomics Viewer was used for visual confirmation of the majority of calls (Thorvaldsdóttir et al., 2013).

CNV Prediction

CNV from sequencing data were profiled using copy number detection by exome sequencing (CODEX) (Jiang et al., 2015). CODEX normalizes depth of coverage using a Poisson latent factor model that removes biases due to GC content, exon capture and amplification efficiency, and latent systemic artifacts. Six Poisson latent factors were included in the normalization model for this dataset, which corresponds to sample- and target-wise biases and artifacts that cannot be directly measured or quantified. Segmentation was restricted to exons for all genes. Only homozygous loss (copy number < 0.7) and high-amplification (copy number > 3.3) calls are reported. Visual confirmation of CNV calls was done in Nexus 7.5 (BioDiscovery) software.

Biostatistical Analysis

RStudio version 1.0.136 was used to analyze the data. One-way ANOVA was used to compare the means of variant calls in cell line, PDX, and PDX CL. Paired t test (along with 95% confidence interval for the difference in means) was used to compare allelic fractions of all variants, the number of all filtered variants among all sample types, the mutational burden between patients that received immunotherapy and naive ones, and mutational burden comparison of naive *NF1* mutants, with other naive subtypes. Chi-square test, Fisher's exact test, or an unpaired t test was used to make other statistical comparisons, as appropriate. For cluster analysis based on correlations, a gene with CNV < 1 or > 1 was selected for data analysis if it was shown from more than 10% of study samples. Spearman correlation coefficients were calculated between each pair of selected genes, and hierarchical clustering by Euclidian distance and complete linkage using the heatmap.2 function available from the R Foundation for Statistical Computing (<http://www.R-project.org>) was further performed to group the genes based on their correlations. For all analyses, $p < 0.05$ was considered statistically significant.

DATA AND SOFTWARE AVAILABILITY

The accession number for the targeted sequencing data reported in this paper is Sequence Read Archive (SRA): SUB2649393.

SUPPLEMENTAL INFORMATION

Supplemental Information includes Supplemental Experimental Procedures, seven figures, and seven tables and can be found with this article online at <https://doi.org/10.1016/j.celrep.2017.10.052>.

AUTHOR CONTRIBUTIONS

C.K., P.B., K.S., M.B., M.X., and B.S. participated in PDX establishment, expansion, banking, and *in vivo* experiments. B.G., I.N.A., B.W., M.A.W., and K.L.N. developed, performed, and analyzed targeted sequencing. X.Y., Q.L., N.M., Y.J., and N.R.Z. performed statistical analysis. W.X., G.K., X.X., R.A., T.C.G., D.E., L.S., J.W., M.A.D., D.T.F., M.B., K.T.F., D.H., M.G., J.B., N.J.P., and C.L.S. performed tissue and clinical data collection. C.K., L.S., M.H., and K.L.N. participated in conception and design of the project. I.N.A., B.G., and K.L.N. wrote the manuscript with input from all authors. K.L.N., C.K., and M.H. supervised the work.

ACKNOWLEDGMENTS

We express our sincere gratitude to the patients who have provided samples for this research. We would like to thank Drs. Takami Sato and Alexander Roesch for sample contribution and Dr. Michal Lotem for providing cell lines M230, M331, and M450. This work was supported by NIH grants P01 CA114046, P01 CA025874, and R01 CA047159 to M.H.; the P50 CA174523 SPORE on Skin Cancer to the Wistar Institute and the University of Pennsylvania; the Melanoma Research Alliance (K.L.N.); philanthropic contributions to the Melanoma Moon Shots Program at the University of Texas MD Anderson Cancer Center; and the Dr. Miriam and Sheldon G. Adelson Medical Research Foundation (D.H., M.H., and M.A.D.).

Received: May 10, 2017

Revised: August 17, 2017

Accepted: October 13, 2017

Published: November 14, 2017

REFERENCES

- Abecasis, G.R., Auton, A., Brooks, L.D., DePristo, M.A., Durbin, R.M., Handsaker, R.E., Kang, H.M., Marth, G.T., and McVean, G.A.; 1000 Genomes Project Consortium (2012). An integrated map of genetic variation from 1,092 human genomes. *Nature* **491**, 56–65.
- Arafah, R., Qutob, N., Emmanuel, R., Keren-Paz, A., Madore, J., Elkahlon, A., Wilmott, J.S., Gartner, J.J., Di Pizio, A., Winograd-Katz, S., et al. (2015). Recurrent inactivating *RASA2* mutations in melanoma. *Nat. Genet.* **47**, 1408–1410.
- Berger, M.F., Hodis, E., Heffernan, T.P., Deribe, Y.L., Lawrence, M.S., Protogopov, A., Ivanova, E., Watson, I.R., Nickerson, E., Ghosh, P., et al. (2012). Melanoma genome sequencing reveals frequent *PREX2* mutations. *Nature* **485**, 502–506.
- Brash, D.E. (2015). UV signature mutations. *Photochem. Photobiol.* **91**, 15–26.
- Cancer Genome Atlas Network (2015). Genomic Classification of Cutaneous Melanoma. *Cell* **161**, 1681–1696.
- Cerami, E., Gao, J., Dogrusoz, U., Gross, B.E., Sumer, S.O., Aksoy, B.A., Jacobsen, A., Byrne, C.J., Heuer, M.L., Larsson, E., et al. (2012). The cBio cancer genomics portal: an open platform for exploring multidimensional cancer genomics data. *Cancer Discov.* **2**, 401–404.
- Chapman, P.B., Hauschild, A., Robert, C., Haanen, J.B., Ascierto, P., Larkin, J., Dummer, R., Garbe, C., Testori, A., Maio, M., et al.; BRIM-3 Study Group (2011). Improved survival with vemurafenib in melanoma with *BRAF* V600E mutation. *N. Engl. J. Med.* **364**, 2507–2516.
- Cirenajwis, H., Lauss, M., Ekedahl, H., Törngren, T., Kvist, A., Saal, L.H., Olsson, H., Staaf, J., Carneiro, A., Ingvar, C., et al. (2017). *NF1*-mutated melanoma tumors harbor distinct clinical and biological characteristics. *Mol. Oncol.* **11**, 438–451.
- Corrie, P., Hategan, M., Fife, K., and Parkinson, C. (2014). Management of melanoma. *Br. Med. Bull.* **111**, 149–162.
- Davies, H., Bignell, G.R., Cox, C., Stephens, P., Edkins, S., Clegg, S., Teague, J., Woffendin, H., Garnett, M.J., Bottomley, W., et al. (2002). Mutations of the *BRAF* gene in human cancer. *Nature* **417**, 949–954.
- Dentici, M.L., Sarkozy, A., Pantaleoni, F., Carta, C., Lepri, F., Ferese, R., Correddu, V., Martinelli, S., Briuglia, S., Digilio, M.C., et al. (2009). Spectrum of

- MEK1 and MEK2 gene mutations in cardio-facio-cutaneous syndrome and genotype-phenotype correlations. *Eur. J. Hum. Genet.* **17**, 733–740.
- DePristo, M.A., Banks, E., Poplin, R., Garimella, K.V., Maguire, J.R., Hartl, C., Philippakis, A.A., del Angel, G., Rivas, M.A., Hanna, M., et al. (2011). A framework for variation discovery and genotyping using next-generation DNA sequencing data. *Nat. Genet.* **43**, 491–498.
- Garrison, E., and Marth, G. (2012). Haplotype-based variant detection from short-read sequencing. *arXiv*, arXiv:1207.3907, <https://arxiv.org/abs/1207.3907>.
- George, E., Kim, H., Krepler, C., Wenz, B., Makvandi, M., Tanyi, J.L., Brown, E., Zhang, R., Brafford, P., Jean, S., et al. (2017). A patient-derived-xenograft platform to study BRCA-deficient ovarian cancers. *JCI Insight* **2**, e89760.
- Hauschild, A., Grob, J.J., Demidov, L.V., Jouary, T., Gutzmer, R., Millward, M., Rutkowski, P., Blank, C.U., Miller, W.H., Jr., Kaempgen, E., et al. (2012). Dabrafenib in BRAF-mutated metastatic melanoma: a multicentre, open-label, phase 3 randomised controlled trial. *Lancet* **380**, 358–365.
- Heidorn, S.J., Milagre, C., Whittaker, S., Noury, A., Niculescu-Duvas, I., Dhomen, N., Hussain, J., Reis-Filho, J.S., Springer, C.J., Pritchard, C., and Marais, R. (2010). Kinase-dead BRAF and oncogenic RAS cooperate to drive tumor progression through CRAF. *Cell* **140**, 209–221.
- Helming, K.C., Wang, X., Wilson, B.G., Vazquez, F., Haswell, J.R., Manchester, H.E., Kim, Y., Kryukov, G.V., Ghandi, M., Aguirre, A.J., et al. (2014). ARID1B is a specific vulnerability in ARID1A-mutant cancers. *Nat. Med.* **20**, 251–254.
- Hiemenz, M.C., Kadauke, S., Lieberman, D.B., Roth, D.B., Zhao, J., Watt, C.D., Daber, R.D., and Morrisette, J.J. (2016). Building a robust tumor profiling program: Synergy between next-generation sequencing and targeted single-gene testing. *PLoS ONE* **11**, e0152851.
- Hobbs, G.A., Der, C.J., and Rossman, K.L. (2016). RAS isoforms and mutations in cancer at a glance. *J. Cell Sci.* **129**, 1287–1292.
- Hodis, E., Watson, I.R., Kryukov, G.V., Arold, S.T., Imielinski, M., Theurillat, J.P., Nickerson, E., Auclair, D., Li, L., Place, C., et al. (2012). A landscape of driver mutations in melanoma. *Cell* **150**, 251–263.
- Hoek, K.S., Schlegel, N.C., Brafford, P., Sucker, A., Ugurel, S., Kumar, R., Weber, B.L., Nathanson, K.L., Phillips, D.J., Herlyn, M., et al. (2006). Metastatic potential of melanomas defined by specific gene expression profiles with no BRAF signature. *Pigment Cell Res.* **19**, 290–302.
- Jiang, Y., Oldridge, D.A., Diskin, S.J., and Zhang, N.R. (2015). CODEX: a normalization and copy number variation detection method for whole exome sequencing. *Nucleic Acids Res.* **43**, e39.
- Johnson, D.B., Menzies, A.M., Zimmer, L., Eroglu, Z., Ye, F., Zhao, S., Rizos, H., Sucker, A., Scolyer, A.A., Gutzmer, R., et al. (2015). Acquired BRAF inhibitor resistance: A multicenter meta-analysis of the spectrum and frequencies, clinical behaviour, and phenotypic associations of resistance mechanisms. *Eur. J. Cancer* **51**, 2792–2799.
- Kim, K.H., Kim, W., Howard, T.P., Vazquez, F., Tsherniak, A., Wu, J.N., Wang, W., Haswell, J.R., Walensky, L.D., Hahn, W.C., et al. (2015). SWI/SNF-mutant cancers depend on catalytic and non-catalytic activity of EZH2. *Nat. Med.* **21**, 1491–1496.
- Kim, D.W., Haydu, L.E., Joon, A.Y., Bassett, R.L., Jr., Siroy, A.E., Tetzlaff, M.T., Routbort, M.J., Amaria, R.N., Wargo, J.A., McQuade, J.L., et al. (2017). Clinicopathological features and clinical outcomes associated with TP53 and BRAF(N)(on-)(V)(600) mutations in cutaneous melanoma patients. *Cancer* **123**, 1372–1381.
- Krauthammer, M., Kong, Y., Ha, B.H., Evans, P., Bacchiocchi, A., McCusker, J.P., Cheng, E., Davis, M.J., Goh, G., Choi, M., et al. (2012). Exome sequencing identifies recurrent somatic RAC1 mutations in melanoma. *Nat. Genet.* **44**, 1006–1014.
- Krauthammer, M., Kong, Y., Bacchiocchi, A., Evans, P., Pornputtapong, N., Wu, C., McCusker, J.P., Ma, S., Cheng, E., Straub, R., et al. (2015). Exome sequencing identifies recurrent mutations in NF1 and RASopathy genes in sun-exposed melanomas. *Nat. Genet.* **47**, 996–1002.
- Krepler, C., Xiao, M., Sproesser, K., Brafford, P.A., Shannan, B., Beqiri, M., Liu, Q., Xu, W., Garman, B., Nathanson, K.L., et al. (2016). Personalized preclinical trials in BRAF inhibitor-resistant patient-derived xenograft models identify second-line combination therapies. *Clin. Cancer Res.* **22**, 1592–1602.
- Krepler, C., Sproesser, K., Brafford, P., Beqiri, M., Garman, B., Xiao, M., Shannan, B., Watters, M., Perego, M., Zhang, G., et al. (2017). A comprehensive patient-derived xenograft collection representing the heterogeneity of melanoma. *Cell Reports* **21**, this issue, 1953–1967.
- Lai, Z., Markovets, A., Ahdesmaki, M., Chapman, B., Hofmann, O., McEwen, R., Johnson, J., Dougherty, B., Barrett, J.C., and Dry, J.R. (2016). VarDict: a novel and versatile variant caller for next-generation sequencing in cancer research. *Nucleic Acids Res.* **44**, e108.
- Larkin, J., Chiarion-Sileni, V., Gonzalez, R., Grob, J.J., Cowey, C.L., Lao, C.D., Schadendorf, D., Dummer, R., Smylie, M., Rutkowski, P., et al. (2015). Combined Nivolumab and Ipilimumab or Monotherapy in Untreated Melanoma. *N. Engl. J. Med.* **373**, 23–34.
- Lek, M., Karczewski, K.J., Minikel, E.V., Samocha, K.E., Banks, E., Fennell, T., O'Donnell-Luria, A.H., Ware, J.S., Hill, A.J., Cummings, B.B., et al.; Exome Aggregation Consortium (2016). Analysis of protein-coding genetic variation in 60,706 humans. *Nature* **536**, 285–291.
- Li, H., and Durbin, R. (2009). Fast and accurate short read alignment with Burrows-Wheeler transform. *Bioinformatics* **25**, 1754–1760.
- Lin, W.M., Baker, A.C., Beroukhi, R., Winckler, W., Feng, W., Marmion, J.M., Laine, E., Greulich, H., Tseng, H., Gates, C., et al. (2008). Modeling genomic diversity and tumor dependency in malignant melanoma. *Cancer Res.* **68**, 664–673.
- McKenna, A., Hanna, M., Banks, E., Sivachenko, A., Cibulskis, K., Kernysky, A., Garimella, K., Altshuler, D., Gabriel, S., Daly, M., and DePristo, M.A. (2010). The Genome Analysis Toolkit: a MapReduce framework for analyzing next-generation DNA sequencing data. *Genome Res.* **20**, 1297–1303.
- Rana, A., Rana, B., Mishra, R., Sondarva, G., Rangasamy, V., Das, S., Viswakarma, N., and Kanthasamy, A. (2013). Mixed lineage kinase-c-jun n-terminal kinase axis: a potential therapeutic target in cancer. *Genes Cancer* **4**, 334–341.
- Robert, C., Karaszewska, B., Schachter, J., Rutkowski, P., Mackiewicz, A., Stroiakovski, D., Lichinitser, M., Dummer, R., Grange, F., Mortier, L., et al. (2015). Improved overall survival in melanoma with combined dabrafenib and trametinib. *N. Engl. J. Med.* **372**, 30–39.
- Ryerson, A.B., Ehemann, C.R., Altekruze, S.F., Ward, J.W., Jemal, A., Sherman, R.L., Henley, S.J., Holtzman, D., Lake, A., Noone, A.M., et al. (2016). Annual Report to the Nation on the Status of Cancer, 1975–2012, featuring the increasing incidence of liver cancer. *Cancer* **122**, 1312–1337.
- Tentler, J.J., Tan, A.C., Weekes, C.D., Jimeno, A., Leong, S., Pitts, T.M., Arcaroli, J.J., Messersmith, W.A., and Eckhardt, S.G. (2012). Patient-derived tumour xenografts as models for oncology drug development. *Nat. Rev. Clin. Oncol.* **9**, 338–350.
- Thorvaldsdóttir, H., Robinson, J.T., and Mesirov, J.P. (2013). Integrative Genomics Viewer (IGV): high-performance genomics data visualization and exploration. *Brief. Bioinform.* **14**, 178–192.
- Wagle, N., Van Allen, E.M., Treacy, D.J., Frederick, D.T., Cooper, Z.A., Taylor-Weiner, A., Rosenberg, M., Goetz, E.M., Sullivan, R.J., Farlow, D.N., et al. (2014). MAP kinase pathway alterations in BRAF-mutant melanoma patients with acquired resistance to combined RAF/MEK inhibition. *Cancer Discov.* **4**, 61–68.
- Wang, K., Li, M., and Hakonarson, H. (2010). ANNOVAR: functional annotation of genetic variants from high-throughput sequencing data. *Nucleic Acids Res.* **38**, e164.
- Yao, Z., Torres, N.M., Tao, A., Gao, Y., Luo, L., Li, Q., de Stanchina, E., Abdel-Wahab, O., Solit, D.B., Poulikakos, P.J., and Rosen, N. (2015). BRAF mutants evade Erk-dependent feedback by different mechanisms that determine their sensitivity to pharmacologic inhibition. *Cancer Cell* **28**, 370–383.
- Zhang, T., Dutton-Regester, K., Brown, K.M., and Hayward, N.K. (2016). The genomic landscape of cutaneous melanoma. *Pigment Cell Melanoma Res.* **29**, 266–283.